

Final Report

**Evaluation of the Potential for Cross Contamination of the Edwards Aquifer
from Dissolved Contaminants in the Shallow Groundwater Zone
in the Vicinity of Kelly AFB via Faults and Wells**

by

Susan D. Hovorka, Jeffrey G. Paine, Robert C. Reedy,
Edward W. Collins, and Adrien Lindley

Bureau of Economic Geology
Scott W. Tinker, Director
John A. and Katherine G. Jackson School of Geosciences
The University of Texas at Austin

July 2002

TABLE OF CONTENTS

Executive Summary	1
1.0 Introduction	2
2.0 Geologic and Hydrologic Setting.....	3
2.1 Overview of hydrostratigraphy	3
2.2 Edwards aquifer	3
2.3 Aquitard: Del Rio, Buda, Eagle Ford Formations, Austin Chalk, Taylor Marl, and Navarro Group ...	4
2.4 Alluvium.....	4
2.5 Tectonic history	5
3.0 Methods	6
3.1 Pathways evaluation: Methods used to search for suspected sites of wells using historical photographs	6
3.2 Pathways evaluation: Methods of assessment of geophysical tools that could be used to locate unidentified wells.....	7
3.3 Pathways evaluation: Methods of analysis of faults and fractures through the aquitard as potential pathways	7
3.4 Transport mechanisms: Methods of gradient assessment	8
3.4.1 Water-level elevation in the shallow groundwater zone	8
3.4.2 Water-level elevation in the Edwards aquifer	8
3.4.3 Gradient mapping	10
3.5 Methods of assessment of wells as conduits	10
4.0 Results	10
4.1 Pathways evaluation: Results of search for suspected sites of wells using historical photographs	10
4.2 Pathways evolution: Results of assessment of geophysical tools that could be used to locate unidentified wells.....	11
4.3 Pathways evaluation: Results of analysis of faults and fractures through the aquitard as flow paths.	12
4.4 Transport mechanisms: Results of gradient assessment	14
4.4.1 Water levels in the Edwards aquifer	14
4.4.2 Water levels in the shallow groundwater zone	14
4.4.3 Calculating gradient.....	14
4.5 Results of assessment of wells as conduits	15
5.0 Discussion.....	18
5.1 Evaluation of pathways.....	18
Evaluation.....	20
References Cited.....	21
Appendix 1. Alternate Solution to 4.5 <i>Results of Assessment of Wells as Conduits</i>	23

TABLES

1. Discharge estimates for different pipe diameters and head differences in a smooth, 800-ft pipe.....	16
2. Aqueous diffusion coefficients for selected organic compounds	17

FIGURES

1. Generalized location of Kelly Air Force Base and east Kelly. Major roads and creeks from Texas Department of Transportation via Texas Natural Resources Information System. The study area (circle) includes the mapped contaminant plume above the maximum contaminant levels (MCL's) in the shallow groundwater zone. Data from outside the study area were examined as needed to

understand or define relationships inside the study area. The plume outline was derived by Steve Young (HGL) by integrating four dxf files that were provided by Kelly AFB for solvent contours of PCE, TCE, DCE, and VC based on 2001 field data. The MCL's for PCE, TCE, DCE (1,2-cis DCE), and VC are 5 ppb, 5 ppb, 70 ppb, and 2 ppb, respectively. Area of plume with total solvent concentrations above MCL's is drawn by tracing PCE and TCE 5-ppb contours. The 70-ppb DCE and 2-ppb VC contours are within those PCE and TCE contours.

2. Stratigraphic section, modified from Collins (2000). Wilcox and Midway Groups (not shown) crop out in the south part of the study area.
3. Generalized geologic map showing the geometry of surficial deposits and the recharge and transition zones of the Edwards aquifer with respect to the study area. The recharge and transition zones are extracted from digital data (Texas Natural Resource Conservation Commission, 2001), and the distribution of alluvial sediments is excerpted from Collins (2000) and Brown and others (1974).
4. Distribution of known wells (Texas Water Development Board, 2002), showing drilling date, where known. Modern roads, modern Kelly outline, and study area shown for reference.
5. View northeast across the BexarMet Pitluk station showing several potential sources of magnetic noise that might be expected in an urban setting.
6. Photograph of the Geometrics G-858 magnetometer. Cesium vapor sensor is at the left end of the wand.
7. Comparison of magnetic field strength across the south end of the survey area before and after line data were acquired.
8. Water-level elevation in the study area (Texas Water Development Board, 2002) plotted versus Julian day. For comparison, the monthly water-level elevations in the Bexar County monitor well (AY6837203) are plotted on the same scale. The 1954 synoptic survey is shown at the arrow.
9. Historical 1929–1939 land use classification, with 35-m buffer applied, and known well locations (Science Applications International Corporation, 2000).
10. Map showing magnetic field strength at the BexarMet Pitluk station. Locations of features and measurement locations are also shown. Line numbers are displayed at the bottom of the map.
11. Magnetic-field strength along line 3. Line location shown in figure 10.
12. Magnetic-field strength along line 4. Line location shown in figure 10.
13. Magnetic-field strength along line 8. Line location shown in figure 10.
14. Structure map showing interpreted regional faults, elevation of the top of the Edwards, and thickness of the interval from land surface to top of Edwards. Generalized Kelly outline, study area, and cross-section locations are also shown.
15. Potentiometric map on the Edwards high pseudosynoptic water levels. Outlier values not included in the contour are circled. Study area shown for reference. Fresh/saline interface is excerpted from Schultz (1994).
16. Potentiometric map of the Edwards moderate pseudosynoptic water levels. Outlier values not included in the contour are circled. Study area shown for reference. Fresh/saline interface is excerpted from Schultz (1994).

17. Potentiometric map of the Edwards low pseudosynoptic water levels. Outlier values not included in the contour are circled. Study area shown for reference. Fresh/saline interface is excerpted from Schultz (1994).
18. Potentiometric map of the Edwards 1954 synoptic water level. Study area shown for reference. Fresh/saline interface is excerpted from Schultz (1994).
19. Potentiometric maps of the three synoptic surveys of the shallow groundwater zone. Data extracted from AFBCA Environmental Resources Program Information Management System (ERPIMS) (unpublished digital data, 2002). Study area shown for reference. Synoptic 6 was collected March 3 to March 28, 1998, and represents a generally low level; synoptic 7 was collected March 12 to April 5, 1999, during relatively high level of both aquifers; and synoptic 9, collected March 2 to March 22, 2001, extends over the largest area and is at moderate aquifer level.
20. Water levels for representative wells completed in the shallow groundwater zone plotted versus calendar day. For comparison, the monthly water-level elevation in the Bexar County monitor well (AY6837203) is plotted on the same scale.
21. Calculated hydraulic gradient between the shallow groundwater zone and the Edwards aquifer for high, moderate, low, and 1954 stages. Generalized Kelly outline shown for reference.
22. Relative organic compound solute concentration with time at the end of an 800-ft-length pipe with diffusion as the only transport mechanism.
23. Residual magnetic field strength recorded west of Sterling City, Texas, in September 2001. Data acquired by towing a magnetometer at a height of 73 m with a fixed-wing aircraft flying at a height of 120 m. Data were acquired along north-south lines spaced 100 m apart. (b) Location of active and abandoned oil and gas wells superimposed on residual magnetic field strength. Flight line 225 (fig. 24) passes within 20 m of the shown location of an abandoned oil well.
24. Normalized magnetic field strength along flight line 225 near Sterling City, Texas. Also shown is the position of an abandoned oil well projected onto the flight line.

ATTACHMENTS

- Plate 1. Cross section A–A in pocket
 Plate 2. Cross section B–B..... in pocket

EXECUTIVE SUMMARY

Shallow groundwater in alluvial sediments in southwest San Antonio has been impacted by urban and industrial activities. The shallow groundwater zone overlies an interval characterized as an aquitard, which in turn overlies the Edwards aquifer. The Edwards aquifer is a highly transmissive hydrologic unit that supplies drinking water to the city of San Antonio, as well as diverse other users down gradient. The purpose of this study is to assess the risk that contaminated water can move across the aquitard from the shallow groundwater zone into the Edwards aquifer. The study area is defined by a polygon that includes the Kelly Air Force Base, east Kelly area, and the contaminant plumes mapped by Miller (2000).

The most significant conditions with potential to transmit contaminants from the shallow groundwater zone to the Edwards exist at times when hydrologic gradient is present between the two zones and at places where a pathway having significant permeability connects them. In this study, we assessed the hydraulic gradient between the shallow groundwater zone and the Edwards aquifer. We analyzed faults and water wells as potential pathways having significant permeability through the aquitard.

The gradient between the Edwards and the shallow groundwater in the study area varies spatially and temporally. Likelihood of downward hydraulic gradient is suggested over the northwestern half of the study area during the lowest 25% of water levels in the Edwards aquifer. During average and high water levels in the Edwards aquifer, there is no downward gradient between the shallow groundwater and the Edwards in the study area.

The aquitard between shallow groundwater and the Edwards in the study area ranges from 850 to 1,390 feet thick and is cut by faults having throws of 40 to 140 feet. Structural analysis shows that larger faults are likely to extend from the base of the alluvium that hosts the shallow groundwater through the Edwards. Zones of abundant fractures having no displacement are likely to be associated with these faults. Literature review suggests that the faults and associated fractures are unlikely to have high transmissivity, although mineralization along fractures suggests that fluid flow has been focused along fractures, indicating somewhat higher permeability in the fractures than the matrix.

At times when hydraulic gradient exists, improperly constructed wells have potential to provide an effective pathway for contaminants to flow between the shallow groundwater zone and the underlying Edwards aquifer. Other transport processes such as diffusion are shown to be negligible and can be discounted. This study follows up on previous work inventorying known wells (Science Applications International Corporation, 2000) by investigating methods that can be used to search for previously unidentified wells. We analyzed the historical development of the area to identify sites where wells were likely to have been drilled, for example, isolated farmhouses. However, this method was unsuccessful because of the complex evolution of water use in the area.

We demonstrated the use of a magnetometer survey to identify well casings in an urban area. In the pilot area, the magnetometer survey was successful in locating three large-diameter steel-cased wells and separating the signal produced by the wells from most of the metal on the surface. The signal produced by buildings and surface metal

could be separated on the basis of magnetic field intensity from well casings. A stack of metal pipe produced one false positive. Large metal masses would require additional analysis such as aerial photograph inspection and site visits to separate them from wells. Costs for doing a large-scale airborne magnetometer survey were estimated. Follow-up field-checking would further increase costs.

1.0 INTRODUCTION

Shallow groundwater in alluvial sediments in southwest San Antonio has been impacted as a result of urban and industrial activities, including those at Kelly Air Force Base (AFB). The purpose of this study is to assess the risk that impacted water can move through wells or through faults or fractures from the shallow groundwater zone into the Edwards aquifer, which is the principal regional aquifer at depth.

The area covered by this study is defined as a circle that includes Kelly AFB and East Kelly area and the mapped contaminant plume in the shallow groundwater zone east of the Kelly areas (fig.1). Data from an approximately 10-mile by 10-mile area around this circle was examined as needed to understand or define relationships inside the study area.

This study assesses the possibility that dissolved contaminant could migrate downward into the Edwards aquifer from dissolved phase contamination in the shallow groundwater zone in the defined study area. This analysis included an assessment of pathways and an assessment of transport mechanisms. Two pathways having potential to transport contaminated water are investigated: (1) unidentified and improperly cased wells and (2) faults and associated fracture systems. Transport mechanisms assessed include flow and diffusion.

We analyzed vintage aerial photographs for evidence of distribution of wells prior to intensive development and before public water supply served the area to attempt to locate sites of possible unidentified wells. The concept behind this search is that isolated houses are likely to have had their own water supply, and older wells serving these houses are at higher risk of having not been recorded or not being constructed to current aquifer protection standards.

Geophysical methods are commonly used to locate subsurface features such as unidentified well casings. All geophysical methods require a contrast in some physical property between the feature of interest and its surroundings. The geophysical contrast most likely to be observed around water wells having steel casings is alteration of the local magnetic field. This alteration in magnetic field may be detected using sensitive magnetometers carried either on the ground or by low-flying aircraft. To examine the feasibility of using magnetometers to locate unknown water wells, we conducted a magnetometer survey of a small area near Kelly AFB. The magnetic signature of wells is well known from previous studies; however, the contrast of urban infrastructure such as buildings, near-surface pipelines, fences, and other metallic materials having well signatures was not known. We selected the locations of three wells where other metallic cultural features were present that might mask the well locations.

To determine the continuity and geometry of aquitards beneath the contaminated shallow aquifer, structural surface-to-Edwards cross sections and maps across faults that

cut the area of interest were prepared and the hydrologic implications of these cross sections assessed.

We defined the hydraulic gradient between the Edwards aquifer and the shallow groundwater zone. We considered features such as cones of depression near pumping centers and impacts of fault barriers on water-level response, as well as the impact of the highly variable water levels in the Edwards aquifer on gradient.

We assessed the risk that unknown improperly plugged wells will transmit contaminated water from the shallow groundwater zone to the Edwards aquifer. We calculated the maximum impact of flow through open well bores because of hydraulic gradient. We calculated the impact of other transport mechanisms (for example diffusion) through water-filled well bores.

2.0 GEOLOGIC AND HYDROLOGIC SETTING

2.1 Overview of hydrostratigraphy

The shallow groundwater zone overlies an interval characterized as an aquitard that, in turn, overlies the Edwards aquifer (fig. 2). These units have been described in numerous publications; however, the general characteristics and relevant features are briefly reviewed here and a few key references to the literature cited.

2.2 Edwards aquifer

The Edwards aquifer is highly transmissive, fractured and karstic carbonate aquifer, composed mostly of limestone, dolomitic limestone, marl, and argillaceous limestone of the Walnut Formation and Kainer and Person Formations of the Edwards Group. These units were deposited during the Albian (Lower Cretaceous) in shallow marine shelf environments and are about 600 feet thick in the study area (Maclay and Land, 1988; Hovorka and others, 1998). A low-permeability limestone, the Georgetown Formation, overlies, but is commonly not mapped separately from, the Edwards Group and is included within the Edwards aquifer in this report.

The Edwards aquifer serves as a water supply for many users, including urban water supply in the study area and numerous users down gradient, and provides habitat for endangered species at spring discharge points. Because of very high transmissivity, water levels in the Edwards aquifer typically show rapid and high-amplitude variability. Previous numerical models of the Edwards (Maclay and Land, 1988) assigned transmissivities of 25 to 50 ft²/s to the Edwards aquifer beneath most of the study area. A new aquifer model under construction by a team funded by the Edwards Aquifer Authority (EAA) is working with a conduit model, which will include regionally extensive very high transmissivity conduit systems beneath the study area. The exact location and hydrologic properties of these conduits are not well constrained. The Edwards aquifer regionally has a fairly sharp transition between fresh water recharged from the surface and brackish water containing 1,000 to 3,000 mg/L total dissolved solids

at depth. This transition is known as the fresh/saline interface and is mapped (Schultz, 1994) across the study area. The water in the Edwards aquifer southeast of the fresh/saline interface is of lower quality and is not widely used; however, water in this salinity range is protected by regulation. Well penetrations are rare in this part of the aquifer, and hydrologic data are correspondingly sparse; therefore, the 1,000 mg/L total dissolved solids contour is used as the practical limit of Edwards data.

2.3 Aquitard: Del Rio, Buda, Eagle Ford Formations, Austin Chalk, Taylor Marl, and Navarro Group

The aquitard is composed of an interbedded sequence of low-permeability rocks that are described for this report in six stratigraphic units (Collins, 2000) (fig. 2). The Del Rio Formation is composed of claystone and mudstone deposited in open-shelf environments unconformably on top of the Georgetown Formation. The Buda Limestone is a higher energy limestone interval that is sharply overlain by shale, mudstone, siltstone, and flaggy limestone of the Eagle Ford Formation. The middle Cretaceous Cenomanian-Turonian-age Del Rio-Buda-Eagle Ford interval totals 140 to 170 feet in thickness in the study area. Limestones of the Buda Formation can be water bearing and have been used in places for domestic water supply; however, the Del Rio and Eagle Ford are typical clay-rich units that are transmissive only where fractured or deeply weathered in near-surface settings. The overlying 130 feet of the aquitard are the Austin Group, which is mostly chalk with lesser amounts of limestone, marl, and argillaceous limestone deposited during the Coniacian (Late Cretaceous) in a deeply flooded shelf setting. The Austin Chalk in the shallow subsurface can be a fractured water-bearing unit that locally sources springs or serves as a domestic water supply; it also produces oil in the subsurface. The Late Cretaceous-age lower Taylor Marl, 240 to 270 feet thick, is composed of mudstone, claystone, marl, and limestone, and is transmissive only where fractured or weathered. These units were deposited in shelf environments. The upper Taylor Formation, Navarro Group, and Midway Formation are dominated by claystone and mudstone with locally traceable thin siltstone and sandstone beds deposited in shelf and prodelta environments. The upper Taylor Formation and Navarro Group average 620 feet thick in the study area and have low transmissivity typical of shales. The Paleocene (Tertiary) Midway Formation composed of claystone, mudstone, siltstone, and sandstone pinches out to an erosional edge near the south edge of the study area.

2.4 Alluvium

The youngest sediments are alluvium that was deposited during and after valley incision. Regionally these deposits include several alluvial units of different ages and different hydrologic properties (Collins, 2000), including older gravelly alluvium that may be equivalent to the Uvalde gravel, of late Tertiary to Quaternary age, Pleistocene Leona Formation, composed of sand, silt, and gravel, Holocene terrace alluvium composed of gravel, sand, silt, and mud, and modern alluvium composed of gravel, sand, silt, and mud found mostly in active drainageways. These units are mapped regionally on

the basis of geomorphic and textural characteristics (fig. 3) but have not been separated in the subsurface in the Kelly area.

The characteristics of the shallow groundwater zone within this alluvium in the Kelly area were described by Miller (2000, p. 2-1 to 2-2):

Shallow groundwater typically occurs at depths of 10 to 40 feet below ground surface in an unconfined or locally semiconfined water-bearing layer 3 to 15 feet thick. The shallow groundwater zone occurs in alluvial sediments that rest on top of the Navarro Formation and other relatively impermeable units that comprise an aquitard that is more than 1,000 feet thick. Although the saturated zone occurs at the base of recent alluvial deposits, the groundwater distribution is controlled largely by the surface topography of the underlying Navarro Formation. Infiltrating water percolating through the unsaturated zone is effectively prevented from entering the Navarro Formation. Groundwater moves through basal alluvial sediments that are commonly dominated by gravel-rich zones. Some of these gravel zones are relatively coarse-grained and highly permeable, while others contain significant amounts of silt and clay that greatly reduce permeability.

2.5 Tectonic history

Both the Edwards Group and the low-permeability rocks that compose the overlying aquitard were fractured during Balcones faulting. This regional tectonic event, which is thought to have occurred during the Miocene, produced several thousand feet of down-to-the-southeast deformation. Uplift and subsequent erosion exposed the Edwards Group at the surface. Deformation was accommodated by formation of northeast-trending normal fault strands and by dipping and folded strata (Collins, 1995; Collins and Hovorka, 1997). Fault strands are typically complex, including one or more faults that vary in throw along their length. Numerous small-throw faults and associated fractures that lack significant displacement are clustered in fracture zones near large faults, as well as cutting the gently dipping fault blocks between major faults. Deformation was completed prior to deposition of the preserved alluvial sediments, as indicated by nonoffset contacts and terrace elevations.

The nearest Edwards exposure to the study area is about 9 miles north (fig. 3). The exposed Edwards Group forms the recharge zone for the aquifer and is considered by State and local regulatory agencies as an area where water quality protection measures should be focused. The transition zone shown in figure 3 is defined by regulations (TNRCC, 2001) as an area where geologic formations crop out in proximity to and south and southeast of the recharge zone and where faults, fractures, and other geologic features present a possible avenue for recharge of surface water to the Edwards aquifer. The transition zone is 6 miles north of the study area. Surface water in the study area drains south, away from the recharge and transition zones.

3.0 METHODS

The assessment of risk of cross-aquifer contamination includes analysis of potential pathways for cross-aquifer contamination and the transport mechanisms that could move contaminated water from the shallow groundwater zone to the Edwards. Pathways considered include wells and faults. A survey to locate wells has already been completed (fig. 4) (Science Applications International Corporation, 2000); our focus was on assessing methods that might be used to locate wells that have not been reported. We examined historical aerial photographs to look at development patterns and conducted a pilot evaluation of magnetometer survey to measure the impact of metallic surface objects on detection of well casings. The analysis of faults as pathways includes review of fault geometries and an inventory of information on hydraulic conductivity of faults and fractures relevant to this setting. The assessment of transport mechanisms focused on calculating the hydrologic gradient between the aquifers considering the temporal and geographic relationships. In addition, we estimated the magnitude of transport by diffusion through pathways.

3.1 Pathways evaluation: Methods used to search for suspected sites of wells using historical photographs

We acquired two sets of historical aerial photographs. An incomplete set of 1938 photographs from the Texas Natural Resources Information System (TNRIS) archives was photocopied. In order to obtain more complete coverage of the study area, we purchased photomosaics from Tobin International. These photomosaics, reproduced at a scale of 1 inch = 2,000 ft, were compiled from photographs taken in 1929 of the San Antonio West and Terrell Wells quadrangles. The aerial photographs were scanned and then imported into ArcView software (ESRI, Redlands California). They were registered to modern urban cultural features that were downloaded from TNRIS using the extension SmartImage.

We developed a subjective classification of land use to describe the likelihood that the houses on the photographs had their own water supply. Class 1 land use and class 2 land use have very isolated and somewhat isolated houses in rural settings. Class 3 land use is a rural subdivision, mostly a single row of houses along a road. Class 4 land use is assigned to formally developed subdivisions, with orderly streets and tightly packed houses. Class 5 is assigned to uncertain land uses. Polygons for each type of land use were digitized on the aerial photographs in ArcView. We used ArcView to apply a 35-m buffer to the digitized land use polygons to match the wells with the houses because this would match domestic water supply wells within 100 feet of the house with the house.

We compared the distribution of known wells compiled by Science Applications International Corporation (2000) with the historical land use classification to interpret the implications of land use on distribution of water wells. We also checked the accuracy of the Science Applications International Corporation (2000) database against other available data and found it complete as far as existing records. Three additional wells on Kelly AFB are reported by EAA.

3.2 Pathways evaluation: Methods of assessment of geophysical tools that could be used to locate unidentified wells

On March 12, 2002, we tested the ability of a hand-carried magnetometer to detect well casings at Bexar Met's Pitluk station near Kelly AFB. The site was selected to measure the impact of urban and industrial infrastructure and compare the signal produced by well casings to the signal produced by clutter. In addition to the three operating large-diameter water wells, other significant cultural features that could mask the well signature included a metal building, two concrete block structures, an electrical substation in the northwest corner of the survey area, a stack of well casing, a steel well cone, a tower, and two manhole covers (fig. 5). The instrument, a Geometrics G-858 cesium vapor magnetometer (fig. 6), measures the strength of the magnetic field to a precision of 0.02 nanoteslas (nT), or less than 1 part per million at typical ambient field strengths of 40,000 nT or more. We laid out a 40 × 70-m grid covering the station, acquiring data while walking along nine north-south lines spaced 5 m apart. The system measured total field strength at 1-second intervals. We made a total of 1,131 measurements along these transects at a sample interval of 0.5 seconds, translating to about one measurement every 0.5 m (but varying with walking speed). Because the natural magnetic field strength varies throughout the day, we checked for significant field-strength change by acquiring data along the baseline at the south end of the survey area both before and after data were acquired over the grid. We mapped survey corners, structures, wells, and significant ground debris using a GPS receiver and locating these features on the grid.

We produced an image of magnetic-field strength across the survey area by gridding the data using the software ERMMapper. These data were imported into a geographic database and were overlain with locations of site features to examine the magnetic signature of different feature types (wells versus other infrastructure).

Pre- and post-survey baseline data (fig. 7) show there was little change in the magnetic field strength during the 30 minutes required to acquire magnetic data along the nine lines. Small differences evident on the eastern third of the baseline are most likely due to slight track differences in an area having a high magnetic field gradient.

3.3 Pathways evaluation: Methods of analysis of faults and fractures through the aquitard as potential pathways

Structural analysis was based on the ArcView data set and copies of wireline logs that support the published regional top Edwards structure (Collins and Hovorka, 1997). Additional well data were acquired from the well completion reports compiled by Miller (2000) and photocopies of selected SAWS well data contributed by Alvin Schulz (2002, written communication). Well location was reviewed for constancy using similar techniques to those outlined above for step 2, water-level elevation in the Edwards aquifer.

Two cross sections were prepared across the study area and into the surrounding area. We selected wells for which we could locate wireline logs as much as possible so that we could compare fault displacement sandstone and siltstone beds in the Navarro Formation with fault displacement in the Edwards. Vertically exaggerated sections were

prepared to measure offset, and nonexaggerated cross sections were prepared to assess fault geometries.

Structure on top of the Edwards Group was contoured and gridded. Structure on the base of the shallow groundwater zone was not available, so we subtracted the top Edwards elevation grid from the DEM of the area to determine depth to the aquifer. An estimate of 40 feet of alluvium was subtracted to estimate the thickness of the aquitard. A literature review was used to assess the likelihood that the mapped faulting would increase the permeability of the aquitard.

3.4 Transport mechanisms: Methods of gradient assessment

Hydraulic gradient between the shallow groundwater and the deep aquifer can be calculated by subtracting the potentiometric surface elevations. Density differences between these two fresh-water zones with low concentrations of dissolved contaminant are insignificant relative to the uncertainties of water-level measurements in the Edwards. Pathways that might be accessed by any DNAPL are not assessed in this study.

3.4.1 Water-level elevation in the shallow groundwater zone

Water-level elevation data from the shallow groundwater zone used in this study are derived from the AFBCA Environmental Resources Program Information Management System (ERPIMS) database that provided well names, well locations, and water level measurements from 10 synoptic monitoring events, well datums, and water level elevations in feet.

Nine synoptic maps of water levels were produced by parsing the water-level data table into measurements taken during consecutive days, spanning periods of 4 to 25 days. Data were gridded using a TIN algorithm in ArcView and then hand contoured to guide interpolation through areas of less dense data using surface topography. We discounted local small inconsistencies in water level elevation. These slightly generalized maps are similar to somewhat more extensive water level maps provided by Steve Young (HGL, 2002) and are suitable for the comparison to the more poorly controlled Edwards aquifer pseudosynoptics.

3.4.2 Water-level elevation in the Edwards aquifer

Ideally, water-level data from the Edwards aquifer would be available or collected during the same period that the synoptic surveys were collected in the shallow groundwater zone. However, synoptic data for the Edwards aquifer have not been collected at appropriate spatial or temporal frequency to create Edwards synoptic maps to match the shallow groundwater maps. In order to complete the evaluation of gradient, we developed the following method for making pseudosynoptic maps.

Step 1: Compiling water-level database. Historical water-level data for the study area were compiled from available sources. Essentially all of the water-level data were downloaded from online databases (Texas Water Development Board, 2002). We searched water-level records of the EAA and water levels collected during well logging to assure completeness of the database. Well locations were also downloaded from

TWDB well files, relevant data merged and parsed to create Edwards water-level tables, Julian date calculated, and the resulting table imported into ArcView. Well locations were projected into UTM zone 14, and a subset of the Bexar County data from the 10-mile area around the study area was extracted.

Step 2: Data screening for constancy. One of the major difficulties in using historical Edwards water-level data is variable data quality. The following steps were applied to identify suspect data: (1) check constancy of State well numbers for wells that were either misnumbered or miss-spotted, (2) compare land surface elevation on the 30-m U.S. Geological Survey digital elevation model (DEM) downloaded from TNRIS at the well location with land surface elevation in database, (3) inspect well owner names and information for obvious inconsistencies, and (4) question statistical outliers in water level. Inconsistencies of less than 10 feet in recorded and DEM elevation are common. These small inaccuracies are attributed to inaccuracies in measuring or estimating land surface elevation, limits of precision of elevation in the DEM, and minor errors in recorded latitude and longitude that are commonly apparent when recorded well locations are compared with aerial photographs or topographic maps. In topographically irregular areas, larger inconsistencies between recorded land surface elevation and DEM are produced by minor location errors; however, these inconsistencies do not necessarily indicate that the recorded water-level elevation is unusable where gradients are low. Therefore, judgment is used to determine when to discount questionable data and the results of the assessment noted in the well database.

Step 3: Integrating data to plot aquifer stage with time. In the selected wells around the study area, this was accomplished by comparing spot water measurements with monthly extracts from the continuous water-level recorder in the Bexar County monitor well J17 (AY 6837203). This monitor well is outside of the study area about 9 miles northeast (fig. 3). A plot of spot water levels in selected wells within the study area versus time shows a very strong similarity to the plot of the Bexar monitor well versus time (fig. 8). It is likely that some temporal lag and elevation variation in water-level response exists between the selected wells and Bexar County monitor well; however, in this case, the effect of discounting this difference is insignificant compared with other uncertainties. Therefore, the trends shown by the monthly water levels in the Bexar County monitor well can be directly used to categorize water levels in the Edwards aquifer in the study area.

Step 4: Constructing pseudosynoptic water-level maps. Following the results of step 3, the monthly records from the Bexar County monitor well were used to define aquifer stages. A cumulative frequency plot of water levels in this well was used to define the low (lowest 25%), moderate (middle 50%), and high (upper 25%) of monthly Edwards water levels. The time periods when the water levels are low, moderate, and high were then used to subdivide the selected wells around the study area into pseudosynoptics. Many of the water levels from the selected wells around the study area date from before the beginning of record collection at the Bexar County monitor well; these data could generally not be used. Selected wells were grouped by date into high, medium, and low water levels, inspected to eliminate outliers, and then gridded using ArcView TIN algorithm, which was then smoothed by hand contouring. Outliers are noted on the maps, and possible explanations for anomalous values considered. Distribution of high-volume pumping wells (greater than 1,000 acre feet per year) was acquired from the Edwards Aquifer Authority (Steve Johnson, EAA, 2002, unpublished

digital communication) to see whether any low values could be explained as a result of local drawdown. In addition, real synoptic data sets were extracted from the TWDB data. The most useful of these was a set of 13 measurements collected near the study area during a 23-day period during the 1954 drought of record (fig. 8).

3.4.3 Gradient mapping

Gradient maps during low, moderate, high, and 1954 water levels were created by gridding contoured water levels for appropriate time periods in ARC/INFO TOPOGRID software and subtracting the grid values for the Edwards water level from shallow-zone water levels in ARC/INFO GRID. Positive values indicated downward gradient and negative values indicated upward gradient.

3.5 Methods of assessment of wells as conduits

Open well bores connecting the shallow groundwater zone to the Edwards aquifer are a proposed mechanism for increasing the transmissivity of the aquitard. Basic hydrologic calculations were used to establish the theoretical maximum contaminant fluxes under a range of hydraulic gradients and the rates that result from diffusion. These calculations provide maximum rates. An alternate method of calculation prepared by Steve Young (HGL, 2002) is attached in Appendix 1. A more sophisticated assessment of rates would require numerical modeling that considered the impact of the transmissivity of the shallow groundwater zone as a factor that limits flux.

4.0 RESULTS

4.1 Pathways evaluation: Results of search for suspected sites of wells using historical photographs

Wells have been drilled over a long history in the study area (fig. 4). An assessment of the earliest known photographs of the area (1929–1939) was undertaken to look for areas that might have a high likelihood of predevelopment wells. However, even in 1929, the study area was characterized by somewhat isolated houses (land use 2) in rural settings (fig. 9). No distinctly isolated farms (land use 1) were recognized. Matching known wells from the well location database (Science Applications International Corporation, 2000) with these houses found only 2 wells within the 35-m buffers of 406 houses mapped, and the use of these wells is not identified in the source database. This mismatch suggests that the initial premise, that the isolated houses would be served by Edwards wells, is in error. Rural subdivision (land use 3) is mostly a single row of houses along a road. Eight wells were associated with the 142 areas mapped as this category. Of these, one is classified as private, one as industrial, and four as public water supply wells, and two are unknown. Class 4 land use is assigned to formally developed subdivisions,

having orderly streets and tightly packed houses. Most wells (35) are in the areas mapped in 1929–1939 as subdivision. However, only nine of these wells are documented as existing before 1939. Fourteen wells, all industrial or public water supply wells, are documented as having been drilled after development.

These complex relationships suggest that the approximately 1,000-foot depth to the Edwards aquifer may have favored early development of community wells or, alternatively, use of the shallow groundwater zone. Also, the high quality of the Edwards aquifer appears to have favored investment in private wells even after municipal water supply wells were in operation. Because of the complex history of well drilling, we are unable to develop trends that could be used to identify areas where early and possibly undocumented wells may have been drilled.

4.2 Pathways evolution: Results of assessment of geophysical tools that could be used to locate unidentified wells

Gridded data from all north-south lines (fig. 10) show that the largest magnetic field changes are spatially correlated to the three wells and the stack of steel well casing at the site. The metal and concrete buildings, electrical substation, large steel cone, and manhole covers have a smaller influence on recorded magnetic field strength despite their proximity to the magnetometer. Detailed profiles from three lines (one directly over a well and two adjacent to one or two wells) illustrate the large effect the wells have on the local magnetic field.

Along line 3, which passes between the western and northern wells, magnetic field strength ranges from about 44,000 to 50,000 nT (fig. 11). A steel tower and a stack of casing located 6 to 14 m west of this line cause a gradual increase in field strength of about 2,000 nT. A small, local increase on this line is also associated with the western well, located about 6 m west of this line. The metal building 6 to 9 m west of the line shows no apparent influence on magnetic field strength at this distance, nor on other lines passing closer to the building. Magnetic field strength gradually increases toward the position of the northern well, located about 5 m east of line 3. The concrete building located 5 to 14 m west of line 3 has no apparent effect on the magnetic field recorded along line 3, although it has a small influence on lines 1 and 2.

Line 4 (fig. 12) passes directly over the northern well pad. Between about 10 and 30 m along the line there appears to remain a subtle increase in magnetic field strength at about the position of the stacked casing and steel tower west of the line. A steel manhole cover 3 m east of the line also produces a small magnetic field change. The northern well is associated with an extremely large magnetic anomaly that increases magnetic field strength more than 20,000 nT at the well itself. Similar extremely large effects also occur along lines 1, 2, and 7, which also pass almost directly over stacked well casing and the western and eastern wells. At the wells, field strength increases to as much as 87,000 nT, revealing the large modification of the local ambient magnetic field that is caused by steel well casing and wellhead equipment.

Several sources of potential magnetic field noise are located along line 8 at the eastern edge of the site (fig. 13). Relatively small but measurable effects are visible adjacent to a steel manhole cover located about 1 m east of the line, the eastern well located about 6 m west of the line, and adjacent to a large steel cone located 2 m west of

the line. The concrete building has no apparent influence on this profile or on line 7, the one that intersects the building.

4.3 Pathways evaluation: Results of analysis of faults and fractures through the aquitard as flow paths

The areas of high-volume flux between the surface and the Edwards aquifer are found where the Edwards Group is at the surface and not through the aquitard. Four springs discharge from the Edwards aquifer in areas where stream valleys intersect outcrops of the Edwards aquifer either along faults (Comal, San Marcos, and Hueco springs) or where the Edwards subcrops beneath alluvial deposits (Leona Springs). No known Edwards springs discharge through the aquitard. Large volumes of recharge enter the aquifer beneath streams that cross the Edwards recharge, and lesser volumes enter the recharge zone along small drainages or uplands zone (Maclay and Land, 1988). However, at least one contamination event is known to have impacted the Edwards aquifer through the aquitard. This occurred in the transition zone (area of thin aquitard and locally or intermittently unconfined Edwards aquifer), at a site known as the West Avenue landfill (unpublished report to Edwards Aquifer Authority, 1984). Contamination (various organic solvents) detected in Edwards wells is attributed to spill in the floor of a quarry in the Austin Chalk that moved 240 feet downward through fractures associated with a fault. In order to assess the potential that contamination from the shallow groundwater zone could move through faults and fractures in the aquitard in the Kelly area, we analyzed the structural setting.

The thickness of the aquitard is between 850 and 1,390 feet in the Kelly area (fig.14). Thickness variation is mostly the result of structural offset on the base of the aquitard and removal of the upper part of the Navarro and overlying units prior to deposition of alluvium. Depositional thickness variation and erosional irregularity on the top play insignificant roles.

Mapping the distribution of faults in the subsurface using well log data is highly interpretive. The fault map created in our earlier study (Collins and Hovorka, 1997) is contoured at 100-foot intervals on the basis of the dominant trends in reported top Edwards elevation. Updating the top Edwards elevation with additional data collected since the previous map was completed and adding elevation data from the well records confirm the previous interpretation. Our interpretation of faults is conservative because we interpret much of the observed variability in the elevation on the top Edwards as a result of regional dip (fig. 14). The Kelly area fault map (Anonymous, 1997) has more faults than the interpretation that we present; however, this fault interpretation is difficult to understand in the context of regional trends. Additional data would most likely reveal more complex structures and numerous smaller throw faults. For example, detailed cross sections through other parts of the Balcones trend show that the Edwards and overlying strata are complexly faulted (Brucks, 1927). Complex fault patterns have also been mapped on detailed cross sections through the BexarMet Artesia station area (A. Schultz, 2002, written communication).

Cross sections across the study area show that the section is cut by faults having throws of 40 to 140 feet (plates 1 and 2). In this study, we particularly wanted to know whether the fault throws decrease in the section above the Edwards. For example, fault

displacement could become bed-parallel (Jones and Ferrill, 1996), or it could be accommodated by folding. However, inferring likely geometries defined by marker beds within the Navarro Formation in the aquitard shows that offset on several faults appears to remain constant through this shale-rich section. Offset cannot be measured in most parts of the faults. Faults most likely extend from the Edwards through the aquitard to the base of the alluvium that hosts the shallow groundwater. Outcrop studies (Hovorka and others, 1998) show that zones of abundant fractures having no displacement are likely to be associated with these faults.

There is no direct evidence of the hydrologic characteristics of fractures in the study area. We therefore conducted a literature review of known properties of faults and joints through shale-rich sections. A large amount of literature exists describing the function of faulted shale seals on hydrocarbon reservoirs, for example, Yeilding and others (1997). In many cases, faulted shales act as seals that prevent the buoyant upward movement of hydrocarbons. Formation of a low-permeability fault gauge created by smearing clay-rich rocks along the fault plane plays a critical role in determining the sealing properties of the fault. The ratio of shale to other lithologies in the aquitard suggests that faults will all be sealing. Throws on faults in the study area are not large enough to offset the 310-foot-thick shale-rich interval of the upper Taylor Group and Navarro Formation.

Literature search documents two environments where fracturing increased permeability in shale-rich sections. In the weathering profile, unloading and weathering can increase aperture on high-angle and bedding-plane fractures in a shale section, enhancing permeability (for example, Bradley, 1993; Yelderman and Alexander, 1996). Geopressure and pressure exerted by hydrocarbons can also cause faults through shales to rupture and serve as fluid conduits (for example, Cartwright, 1994; Finkbeiner and others, 2001). Literature review suggests that stress (either stress release or stress increase) is the factor that opens fractures in shale-rich rocks. The stresses across the aquitard in the Kelly area are produced by head contrasts between the aquifers, which are well below geopressure. Weathering and stress relief are probably significant in the upper part of the aquitard, but the effect is expected to diminish with depth and should not favor opening fractures at depths of several hundred feet into the aquitard.

Mineralization is an indicator of flow on fractures. Mineralization observed along some fractures in slightly sandy shale-rich sections of Balcones faults suggests that at some time fractures had somewhat higher permeability than the matrix. Flow through these low-permeability rocks, however, is commonly local, not cross-formational (for example, Dutton and others, 1994), so mineralization does not necessarily support a model of permeable fractures.

Shale-rich sections are not well known because they crop out only under special conditions, are rarely cored, and are less studied than more economically significant permeable rocks. However, given the current state of knowledge, significant cross-formational flow through faults and associated nonoffset fractures through the aquitard in the study area is not expected.

4.4 Transport mechanisms: Results of gradient assessment

4.4.1 Water levels in the Edwards aquifer

Following the procedure described in section 3 (Methods) to use the Bexar County monitor well to separate the wells near the Kelly area into low, average, and high water levels, water-level maps were developed for each aquifer stage. Because they are pseudosynoptic maps, some wells have more than one water level collected during each stage. These multiple values are posted and provide a variance for the map. Using the results of screening for data consistency, anomalous water levels were identified and not included in the water-level maps. Excluded values are circled on maps.

The potentiometric map of high water levels (fig. 15) shows the expected gradient toward the fresh/saline interface. High water levels are above land surface in the southwestern part of the area, so wells are artesian. Moderate water levels (fig. 16) also show a gradient toward the fresh/saline interface.

The potentiometric map of water levels in the low stage is irregular (fig. 17). This may be the result of the considerable range of water levels incorporated within the low stage. We considered the possibility that some low values were the result of high-volume pumping; however, low values do not match high-volume wells provided by the EAA. We also considered geologic factors such as compartmentalization or conduit development that might explain anomalous water levels; however, no explanation was found. Uncertainty remains about the quality of the data. One reasonably large synoptic data set is available from the 1954 drought of record. The potentiometric map of these data shows a more internally consistent gradient toward the fresh/saline interface (fig. 18).

4.4.2 Water levels in the shallow groundwater zone

Nine synoptic water-level surveys from the AFBCA Environmental Resources Program Information Management System (ERPIMS) database were examined. They show very similar geographic patterns (fig. 19) with high water levels in the northwest decreasing toward discharge points along drainages to the east and south. Representative wells having fairly complete water level records from various parts of the shallow groundwater zone were selected to map fluctuation through time (fig. 20). Variation in water-level elevation in the shallow groundwater zone during the 6-year sampling period is at most wells in the range of 2 to 7 feet, which is small compared with the 57-foot fluctuation in the Edwards monitoring well during the same period. If daily fluctuation for the Edwards were considered or a longer time period considered, the fluctuation in the Edwards would be larger.

4.4.3 Calculating gradient

The gradient between the Edwards and the shallow groundwater in the study area varies spatially and temporally. Figure 20 shows the elevation of the shallow groundwater zone overlain on water level in the Bexar County monitor well. Because the Bexar County monitor well is a proxy for the Edwards wells in the study area (fig. 8), this

relationship approximates the gradient between the shallow aquifer and the Edwards in the study area. No water levels were collected in the shallow groundwater zone during the lowest water levels in the Edwards (fig. 20); however, the suppressed curve of the temporal changes in water levels in the shallow zone suggests that the water levels do not fall to match the lows reached by the Edwards. This plot shows that in most parts of the study area, during high stages Edwards water levels are above those in the shallow groundwater zone, and gradient is upward from the Edwards to the shallow zone. During low water levels, Edwards water levels are below those in the shallow zone, and gradient is downward, with the potential for flow from the shallow groundwater zone downward to the Edwards. During moderate water levels, gradient is generally from the Edwards into the shallow groundwater zone, with the exception of the two representative wells near the groundwater divide south of Kelly AFB.

Better spatial resolution on the distribution of gradient at three aquifer stages is identified by subtracting the gridded water levels at high, moderate, and low stages of the Edwards (fig. 21). Uncertainties are introduced because of the assumptions that were used to create pseudosynoptic potentiometric maps; however, these plots give some idea of the likely distributions of gradient. During high water levels (fig. 21a), the gradient is strongly upward everywhere in the study area. Water would move upward through any permeable connection between the aquifers. During moderate levels (fig. 21b), the gradient is upward, although the gradient is near zero in parts of the study area and small changes in contouring could reverse the results. During low water levels (fig. 21c), gradient is downward in the northwestern part of the study area, although upward gradient persists in the southwest. During the flat, low water levels of the Edwards during the 1954 drought (fig. 21), the area of downward gradient was most likely more extensive. Gradient southeast of the fresh/saline interface is poorly constrained because local information on head in the saline zone is not available. However, regionally head in the saline is similar or slightly higher than in the fresh zone (John Waugh, San Antonio Water System, report on saline zone wells, 2002), so the flat contouring used is reasonable.

4.5 Results of assessment of wells as conduits

Properly completed wells are engineered to prevent cross-contamination of aquifers. Well completion reports on known wells can be inspected to determine that well construction is adequate, idle wells plugged, and in-use wells assessed to ensure that engineering is adequate. However, these assurances cannot be made if a well is not inventoried. The following calculations are presented to determine the maximum risk to the aquifer through an unknown open well between the aquifers. A smooth pipe with a length of 800 feet was assumed for the calculations. Assuming that water flow to and from the pipe is not limited by the hydraulic conductivity or transmissivity of either aquifer, we calculated the flow rate that is possible through the pipe. When the heads of both aquifers are equal, we calculated the effect of diffusion as the mechanism for contaminant transport through the pipe.

Flow rates resulting from different pipe diameters and head differences between the aquifers were investigated. Flow discharge rates were initially estimated using the Poiseuille equation (Pnueli and Gutfinger, 1992):

$$Q = \frac{\pi R^4}{8\mu} \left(-\frac{\Delta P}{\Delta z} \right) \quad (\text{eq. 1})$$

where Q is the discharge rate ($L^3 T^{-1}$), R is the pipe radius (L), μ is the dynamic viscosity of water ($M L^{-1} T^{-1}$), P is pressure ($M L^{-1} T^{-2}$), z is the pipe length (L), and $\Delta P/\Delta z$ is the pressure gradient in the pipe. The negative sign indicates that flow is in the direction of decreasing pressure. Equation 1 is based on the assumption of laminar (nonturbulent) flow. From these results average water flux values were calculated by dividing the Q values by the pipe cross-sectional areas. The Reynolds number (Re , a unitless value expressing the ratio of dynamic to viscous forces) was calculated to determine whether the flux values estimated from eq. 1 resulted in laminar or turbulent flow:

$$Re = \frac{DV}{\nu} \quad (\text{eq. 2})$$

where D is pipe diameter (L), V is average flux ($L T^{-1}$), and ν is kinematic viscosity ($L^2 T^{-1}$) (obtained by dividing the dynamic viscosity, μ , by fluid density). In cases where $Re \leq 2000$, laminar flow is indicated. Calculations using eq. 1 resulted in Re values ranging from 3×10^4 to 1×10^6 , indicating that flow is turbulent and the Poiseuille equation is not valid for estimating discharge. A modified form of the Bernoulli equation was employed to estimate turbulent flux values in the pipe (Pnueli and Gutfinger, 1992):

$$h = \frac{V^2}{2g} \left(1 + f \frac{L}{D} \right) \quad (\text{eq. 3})$$

where V is average flow velocity or flux ($L T^{-1}$), h is head drop in the pipe (L), g is gravitational acceleration ($L T^{-2}$), L is the pipe length (L), D is the pipe diameter (L), and f is the friction factor (unitless). The two unknown values in eq. 3, V and f , were determined iteratively. Values of the friction factor were obtained from a Moody Diagram that relates frictional head loss characteristics for turbulent flow in pipes through successive estimates of Re . The diagrammed curve for a smooth pipe was used for these calculations and resulted in the highest flux values for a given pipe diameter and head difference. Flux values were multiplied by the pipe cross-sectional areas to obtain flow rates. The resulting flow rates for different pipe diameters and head differences are listed in Table 1. At the indicated flow rates, the time required for one complete pipe volume to flow between the aquifers ranges from 1 to 12 minutes.

Pipe Diameter (in)	Discharge (gpm)				
	h = 0 ft	h = 1 ft	h = 5 ft	h = 10 ft	h = 20 ft
4	0	42	104	153	224
8	0	264	645	948	1385
12	0	770	1866	2726	3960

Table 1. Discharge estimates for different pipe diameters and head differences (h) in a smooth, 800-ft-length pipe.

The effectiveness of diffusion as a transport mechanism was investigated using Fick's first law (Fetter, 1993):

$$F = -D \left(\frac{dC}{dx} \right) \quad (\text{eq. 4})$$

where F is the solute mass flux ($M L^{-2} T^{-1}$), D is the solute diffusion coefficient ($L^2 T^{-1}$), C is solute concentration ($M M^{-1}$), and dC/dx is the concentration gradient. The negative sign indicates that mass transport is in the direction of decreasing concentration. The solution to eq. 4 as a function of time, t , and distance, x , with the appropriate boundary conditions of a constant solute concentration of C_0 at $x = 0$ for $t \geq 0$ and $C = 0$ at $x = \infty$ for $t \geq 0$ results in (Fetter, 1993):

$$\frac{C}{C_0} = \text{erfc} \left(\frac{x}{2(Dt)^{0.5}} \right) \quad (\text{eq. 5})$$

where *erfc* is the error function complement. The relative concentration C/C_0 represents the ratio of the concentrations at each end of the pipe, and the results are thus independent of the actual initial concentration. Using a pipe length of 800 ft and selecting an appropriate diffusion coefficient, the relative concentration at the initially zero-concentration end of the pipe as a function of time was determined. The aqueous diffusivity values of several organic compounds commonly encountered as contaminants in groundwater are listed in Table 2. The minimum and maximum values were chosen for these calculations.

Compound	D (cm^2/s at 20°C)	Compound	D (cm^2/s at 20°C)
Toluene	9.0×10^{-6}	Perchloroethylene	9.3×10^{-6}
Xylenes	8.4×10^{-6}	Dichloromethane	1.2×10^{-5}
Benzene	1.0×10^{-5}	Chloroform	1.1×10^{-5}
Ethylbenzene	8.3×10^{-6}	Carbon tetrachloride	9.5×10^{-6}
Chlorobenzene	8.5×10^{-6}	1,1,1-Trichloroethane	9.4×10^{-6}
Trichloroethylene	1.0×10^{-5}		

Table 2. Aqueous diffusion coefficients for selected organic compounds (Pankow and Cherry, 1996, Table 7.8, p. 226)

A graph of the relative solute concentrations versus time calculated using eq. 5 is presented in figure 19. The results indicate that with diffusion as the only transport mechanism, an organic compound listed in table 2 having a concentration of 1,000 ppm would require from 32,800 to 47,500 years before a 1-ppb concentration ($C/C_0 = 10^{-6}$) appeared at the other end of the pipe. Concentrations exceeding 500 ppm ($C/C_0 = 0.5$) would require more than 2 million years to appear at the other end of the pipe.

The assumption that the pipe is smooth and open is likely to be an unrealistic oversimplification, and many scenarios with an inadequate well completion would reduce the transmissivity of the pipe.

The initial assumption, that water flow to and from the pipe is not limited by the hydraulic conductivity or transmissivity of either aquifer, is unrealistic because the shallow groundwater zone has variable saturated thickness and transmissivity (Miller, 2000; Young, 2002, written communication). High and variable transmissivity of the Edwards, modeled as 50 ft²/s (Maclay and Land, 1988) is probably not a limit on pipe flow. An initial assessment of the impact of aquifer properties on the maximum is included as Appendix 1. A more sophisticated analysis built on a hydrologic model of the shallow groundwater zone could quantify the limitations on cross-aquifer contamination that result from local or temporal limits on the productivity of the shallow groundwater zone.

Because of the multiple scales of permeability (matrix, fracture, karst) typical of the Edwards aquifer, it is not practical to attempt to calculate the concentration of contaminant that could be found at a reception site if it were introduced down an unknown well. Dilution is generally very significant in this high-volume, high-velocity aquifer, and mass balance considerations would assure that any amount of contaminant introduced down a single well bore would be diluted before discharging at springs.

5.0 DISCUSSION

5.1 Evaluation of pathways

Wells have been drilled over a long history in the study area. An assessment of the earliest known photographs of the area (1929-1939) failed to clearly match wells with residential and commercial development, suggesting that the depth of the Edwards aquifer may have favored early development of community wells or use of the shallow groundwater zone for domestic water supply. In addition, the high quality of the Edwards aquifer appears to have favored investment in private wells even after municipal water supply wells were in operation. This chaotic well development precludes use of a historical approach to identification of focused areas in which to search for unrecorded wells.

This ground-based magnetometer survey of a small area where well locations are known and potential sources of magnetic field noise are present demonstrates that steel-cased wells (and associated wellhead equipment) produce large magnetic-field anomalies that are detectable using a magnetometer. Further, other sources of magnetic field anomalies either are so large as to be easily distinguishable from wells (stacked casing) or produce very small, local anomalies (manhole covers, metal and concrete buildings, steel surface debris, and small electrical facilities). Despite this success at distinguishing wells from other anomaly sources, a ground-based magnetometer search for unknown, steel-cased wells would be impractical for a large-scale well survey in a residential or industrial area owing to lack of access and numerous along-track impediments for the short line spacing required to detect wells among other sources of noise.

To overcome these difficulties, magnetometers carried by low-flying aircraft (helicopter or fixed wing) have been used to locate oil and gas wells over large areas (for example, Paine and others, 1997, 1999; Wilson and others, 1997). Although magnetic

field strength decreases rapidly with distance from the source, the large mass of steel represented by a cased well produces anomalies that are large enough to be detected using airborne instruments. In a recently completed airborne survey covering 162 km² in Sterling County, Texas, magnetic field data acquired at a line spacing of 100 m were used to compare oil and gas well locations obtained from Texas Railroad Commission databases with magnetic field anomalies detected by the airborne magnetometer. In this survey, the aircraft flew at a height of 120 m, towing a cesium vapour magnetometer at a height of 73 m. Even at the display scale, numerous local anomalies are evident in the geophysical data (fig. 8a). When oil and gas well locations are superimposed on the image (fig. 8b), it is evident that most of the anomalies are associated with one or more well locations. Because of the height of the magnetometer, the magnitude of the anomalies is not as large as that measured using ground-based instruments. For example, line 225 of the Sterling County survey (fig. 24) passed within about 15 m of the plotted location of an abandoned well having no significant surface equipment. This well is associated with a magnetic field anomaly that is large compared with other anomalies along the line (more than 20 nT), but three orders of magnitude smaller than the anomalies associated with the water wells at the Pitluk Station as measured by ground instruments. Similar results have been obtained from oil fields in Runnels and Montague Counties using helicopter-based magnetometers flying at lower heights.

The success of an airborne magnetometer survey is governed by the size of the feature, the strength of the anomaly it produces, the height of the magnetometer above the ground, and the spacing of the survey lines. Typical airborne survey line spacings are 100 m or more, which is sufficient to detect many wells. Wells located between flight lines may not be detected, and clusters of closely spaced wells may appear as a single magnetic anomaly. These potential shortcomings can be addressed (at increased expense) by flying at tighter line spacings, particularly if a helicopter is used to tow the magnetometer.

The relatively large mass of magnetically susceptible material in a cased well to depths of 100 m or more produces much larger anomalies than are produced by most cultural materials present in an urban area. Significant local anomalies that are similar to those produced by a cased well will undoubtedly be detected in an airborne survey, but these "false positives" can commonly be identified through analysis of recent, high-resolution aerial photography. Anomalies that remain after photographic analysis should be field-checked to determine the source of the anomaly. The number of false positives cannot be quantitatively predicted in advance; however, in areas having oil-field infrastructure, airborne magnetics have been successful at separating wells from other equipment (fig 23). False positives would be magnetic features similar to the stack of pipe casing at the BexarMet Pitluk station and not include smaller structures that could be screened out on magnitude of response; however, small-diameter domestic water supply casing would give a weaker response than the demonstration wells. In addition, it would be difficult to identify well casing within other large magnetic anomalies.

Depending on local regulations, it may not be possible to conduct a low-altitude airborne survey over a residential area. Federal Aviation Administration guidelines commonly restrict aircraft altitude in urban areas such that the allowed flight height may be too high to detect anomalies associated with well casings.

Highest risk of downward flow from the shallow groundwater zone into the Edwards is during low stages of the Edwards aquifer. We express greater confidence in the potentiometric map of the 1954 synoptic than the low pseudosynoptic, because the

low values and the irregularity in the low pseudosynoptic are difficult to explain. Uncertainty is also introduced because water levels in the shallow groundwater zone were not measured during the peak of drought. However, the low amplitude of water-level fluctuations of the shallow zone suggested that the volatility because of variation in recharge is low, possibly because of low discharge. Alternatively, natural recharge may be supplemented and stabilized by urban processes such as leaking water supply pipes, irrigation, or wastewater discharge. The impact of production in the shallow groundwater zone during drought has not been assessed, but it will most likely reduce risk of cross-aquifer contamination, especially in areas where the transmissivity or saturated thickness of the shallow groundwater zone is low.

During moderate and high stages in the Edwards, the gradient for flow in the study area is upward. During moderate and high aquifer stages, any improperly completed wells that connect the Edwards with the shallow zone would discharge Edwards water into the shallow zone. This process would be expected to dilute contaminant and lower concentrations around the discharge point, which might provide a method for exploration for undetected wells.

Areas of highest risk for large-volume flux of dissolved contaminant from the shallow groundwater zone to the Edwards aquifer would also be influenced by contaminant concentration and by transmissivity distribution in the shallow groundwater zone. These variables have been assessed in previous studies (Miller, 2000; Young, written communication, 2002) and were not further analyzed in this study.

EVALUATION

The major risk of contamination of the Edwards aquifer by cross-formational transfer of water from the shallow groundwater zone to the Edwards occurs during low water levels in Edwards, because at these times a downward gradient is likely to exist between the aquifers over the northwestern half of the study area. Risk would be highest in areas having highest concentrations of contaminant as well as areas having thick and transmissive alluvium.

Unknown wells are considered to be a more significant risk than flow along fractures. Closely spaced (50-foot flight lines) airborne magnetic survey is assessed as the best available mechanism for looking for unknown wells. If follow-up work to reduce risk from unidentified improperly completed wells is desired, magnetometer surveys at 50-foot line spacing are recommended.

REFERENCES CITED

- Anonymous, 1997, Selected Edwards wells, shallow aquifer concentration in the Kelly Air Force Base area: plate 4D.
- Bradley, R. G., 1993, The hydrology of the Lake Waco Formation (Eagle Ford Group), central Texas: Baylor University, unpublished Master's thesis.
- Brown, T. E., Waechter, N. B., Rose, P. R., and Barnes V. E., 1974, San Antonio sheet: The University of Texas at Austin, Bureau of Economic Geology, Geologic Atlas of Texas, scale 1:250,000.
- Brucks, E. W., 1927, The Luling field, Texas: American Association of Petroleum Geologists, v. 11, p. 638-639.
- Cartwright, J. A., 1994, Episodic basin-wide fluid expulsion from geopressed shale sequences in the North Sea basin: *Geology*, v. 22, p. 447-450.
- Collins, E. W., 1995, Structural framework of the Edwards aquifer, Balcones Fault Zone, Central Texas: Gulf Coast Association of Geological Societies Transactions, v. 45, p. 135-142.
- Collins, E. W., 2000, Geologic map of the New Braunfels, Texas, 30 × 60 minute quadrangle: geologic framework of an urban-growth corridor along the Edwards aquifer, South-Central Texas: The University of Texas at Austin, Bureau of Economic Geology, scale 1:100,000, 28 p.
- Collins, E. W., and Hovorka, S. D., 1997, Structure map of the San Antonio segment of the Edwards aquifer and Balcones Fault Zone, South-Central Texas: Structural framework of a major limestone aquifer: Kinney, Uvalde, Medina, Bexar, Comal and Hays Counties: The University of Texas at Austin, Bureau of Economic Geology, Miscellaneous Map 38, scale 1:250,000.
- Dutton, A. R., Collins, E. W., Hovorka, S. D., Mace, R. E., Scanlon, B. R., and Xiang, Jiannan, 1994, Occurrence and movement of ground water in Austin Chalk and Eagle Ford and Ozan Formations at the Superconducting Super Collider (SSC) site, Ellis County, Texas: The University of Texas at Austin, Bureau of Economic Geology, topical report prepared for the Texas National Research Laboratory Commission under contract no. IAC(92-93)-0301, 393 p.
- Fetter, C.W., 1993, Contaminant hydrogeology: New York, Macmillan Publishing Company, 458 p.
- Finkbeiner, Thomas, Zoback, Mark, Flemings, Peter, and Stump, Beth, 2001, Stress, pore pressure, and dynamically constrained hydrocarbon columns in the South Eugene Island 330 field, northern Gulf of Mexico: American Association of Petroleum Geologists Bulletin, v. 85, p. 1007-1031.
- Hovorka, S. D., Mace, R. E., and Collins, E. W., 1998, Permeability structure of the Edwards aquifer, South Texas—implications for aquifer management: The University of Texas at Austin, Bureau of Economic Geology Report of Investigations No. 250, 55 p.

- Jones, S. M., and Ferrill, David, 1996, Evidence of layer-parallel shear above high-angle normal faults (abs.): Geological Society of America, Abstracts with Programs, v. 28, p. 244.
- Maclay, R. W., and Land, L. F., 1988, Simulation of flow in the Edwards aquifer, San Antonio Region, Texas, and refinements of storage and flow concepts: U.S. Geological Survey Report Water-Supply Paper 2336, 48 p.
- Miller, John K, 2000, Physical and chemical characteristics of the shallow groundwater zone and sources of groundwater contamination in the vicinity of Kelly Air Force Base, Texas, Volume 1: Analysis and recommendations, final draft Mitretek Technical Report MTR 2000-10-1, variably paginated.
- Paine, J. G., Dutton, A. R., and Blüm, M. U., 1999, Using airborne geophysics to identify salinization in West Texas: The University of Texas at Austin, Bureau of Economic Geology, Report of Investigations No. 257, 69 p.
- Paine, J. G., Dutton, A. R., Mayorga, J. S., and Saunders, G. P., 1997, Identifying oil-field salinity sources with airborne and ground-based geophysics: a West Texas example: *The Leading Edge*, v. 16, no. 11, p. 1603–1607.
- Pankow, J. F., and Cherry, J. A., 1996. Dense chlorinated solvents and other DNAPLs in Groundwater: Guelf, Ontario, Waterloo Press, 522 p.
- Pnueli, D., and Gutfinger, C., 1992. Fluid mechanics: Cambridge University Press, 482 p.
- Schultz, A. L., 1994, 1994 review and update of the position of the Edwards aquifer freshwater/saline-water interface from Uvalde to Kyle, Texas: Edwards Underground Water District report 94-05, 31 p.
- Science Applications International Corporation, 2000, Location of Edwards aquifer wells in plume areas from East Kelly and Kelly Air Force Base: Contract report to San Antonio Air Logistics Center, Directorate of Environmental management, Kelly Air Force Base, Contract No. F41650-95-D-2004-5029, variably paginated.
- Texas Natural Resource Conservation Commission, 2001, Edwards Aquifer Recharge Zone - Chapter 213 Rules (UTM Version), www.tnrcc.state.tx.us/gis/metadata/edw_utm27_met.html#Spatial_Data
- Texas Natural Resources Information System (TNRIS), 2002, <http://www.tnr.is.state.tx.us/digital.htm>
- Texas Water Development Board, 2002, digital data for Bexar County: <http://www.twdb.state.tx.us/publications/reports/GroundWaterReports/GWDatabaseReports/GWdatabaserpt.htm>: well data table and water level table.
- Wilson, C. R., Tsoflias, G., Bartelmann, M., 1997, A high precision aeromagnetic survey near the Glen Hummel field in Texas; identification of cultural and sedimentary anomaly sources: *The Leading Edge*, v. 16, no. 1, p. 37–42.
- Yeilding, Graham, Freeman, Brett, and Needham, D. T., 1997, Quantitative fault seal prediction: *American Association of Petroleum Geologists Bulletin*, v. 81, p. 897–917.
- Yelderman, J. C. and Alexander, Russ, 1996, The relationships between fractures in outcrops and cores as they relate to weathering, geomorphology, hydraulic conductivity, and flow directions in shales at a landfill scale (abs.): Geological Society of America, Abstracts with Programs, v. 28, p. 75.

APPENDIX 1.

Alternate Solution to 4.5 Results of Assessment of Wells as Conduits

Prepared by Steve Young, HGL

Accurate estimates of flow through an abandoned well connecting two aquifers with different hydraulic heads is a highly nonlinear problem that is best solved using a numerical groundwater model. Within the groundwater literature there are several analytical models that can be used to provide a level of magnitude estimate of the flow that would occur between these two wells. For the purpose of this study we have opted to use the analytical model presented by Silliman and Higgins (1990) in their paper titled "An Analytical Solution for Steady-State Flow Between Aquifers Through an Open Well."

Details of the paper by Silliman and Higgins (1990) are beyond the scope of this study, but a brief overview is presented for the interested reader. The analytical solution solves a simplified set of equations for vertical flow in a single well that penetrates two aquifers separated by an aquitard. Head loss associated with flow to (or away) from the well in the upper aquifer and lower aquifer is estimated on the basis of the classical Thiem Equation. Head loss that occurs as a result of water entering and flowing vertically in the well is assumed to be proportional to the square of the flow (Jacob, 1946; Bear, 1979) and is thereby represented by:

$$H_{\text{wellloss}} = CQ^2$$

Where Q is the maximum vertical flow through the well and C is a well-loss constant.

Application of the Silliman and Higgins (1990) analytical solution requires an estimate of the aquifer transmissivities, radius-of-influences associated with the induced flow in both aquifers, effective well radius, and the hydraulic head values at the radius-of-influence in both aquifers. For this analysis, the transmissivity value of approximately 5,000,000 ft²/day was used for the Edwards aquifer. The transmissivity values of 100 ft²/day and 5000 ft²/day were used for the saturated deposits above the Navarro Clay. These transmissivity values were taken from the area in Figure 1 that corresponds to where downward hydraulic gradients may occur. Figure 1 is a map of transmissivities calculated by HydroGeoLogic on the basis of March 2001 water table information.

Parameters for the analytical model besides the transmissivity values were estimated on the basis of very limited data. Considerable uncertainty is associated with these model parameters. In order to err on the side of environmental protection, the estimates for the model parameters were strongly biased to values that would err on the overestimation of the vertical flow. The parameter values used for the final model calculations include a well coefficient of 1x10⁻¹¹ dy²/ft⁵, a 5-foot radius-of-influence in the upper aquifer, and a 50-foot radius-of-influence in the lower aquifer.

Table 1 shows the range of calculated flows based on a range of assumptions concerning the well diameter and the head difference between the terrace deposits and the Edwards aquifer.

Table 1:

Calculated vertical flow (gpm) through a well that connects the saturated terrace deposits to the Edwards aquifer as a function of the transmissivity of the terrace deposits, the diameter of the well, and the head difference between the two aquifers.

Transmissivity ft ² /day	1 ft. Head Difference			5 ft. Head Difference			10 ft. Head Difference			20 ft. Head Difference		
	4"OD	8"OD	12"OD	4"OD	8"OD	12"OD	4"OD	8"OD	12"OD	4"OD	8"OD	12"OD
100	0.05	0.06	0.07	1	2	2	5	6	7	19	24	28
5000	2	3	4	60	75	89	240	302	355	961	1206	1418

Bear, Jacob, 1979, *Hydraulics of groundwater*: New York, McGraw-Hill, 569 p.

Jacob, C. E., 1946, Radial flow in a leaky artesian aquifer: *American Geophysical Union Transactions*, v. 27, no. 2, p. 198–208.

Silliman, Stephen and Higgins, David, 1990, An analytical solution for steady-state flow between aquifers through an open well: *Groundwater*, v. 28, no. 2 p. 184–190.

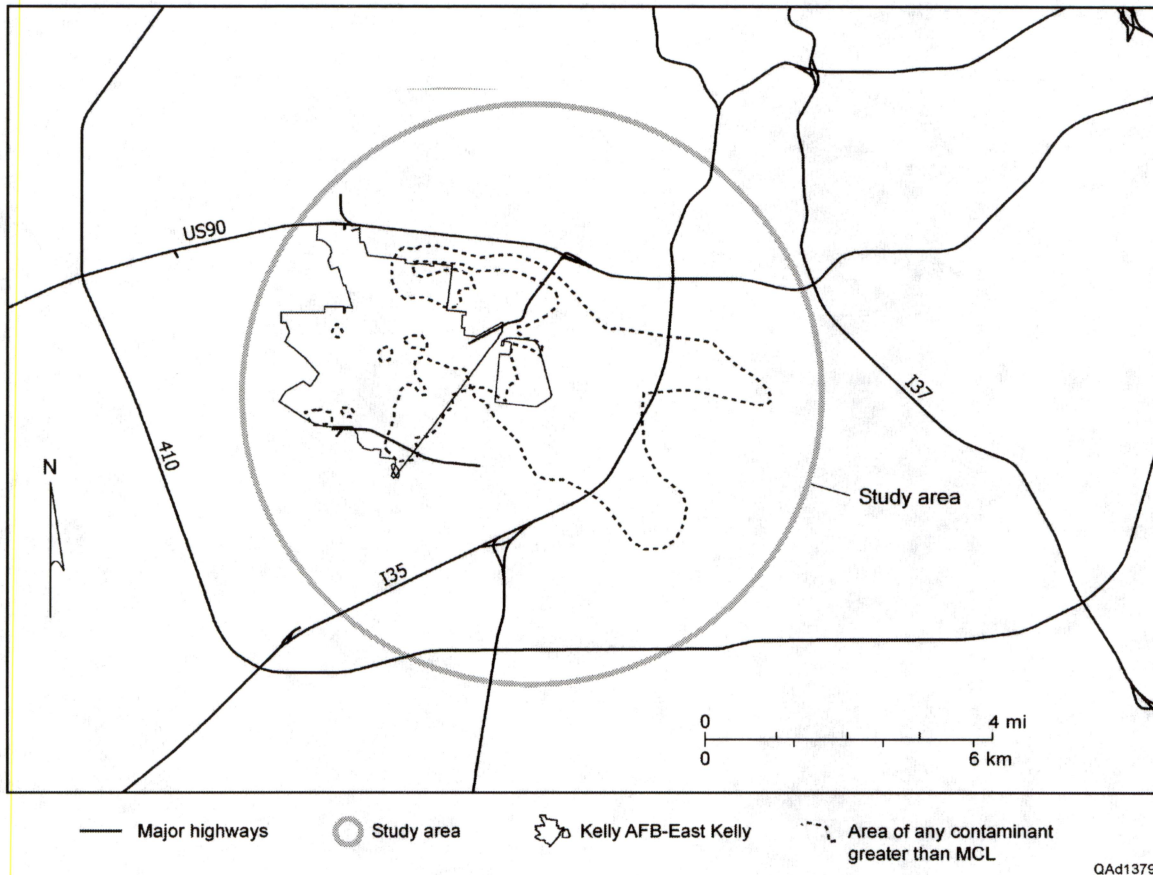


Figure 1. Generalized location of Kelly Air Force Base and east Kelly. Major roads and creeks from Texas Department of Transportation via Texas Natural Resources Information System. The study area (circle) includes the mapped contaminant plume above the maximum contaminant levels (MCL's) in the shallow groundwater zone. Data from outside the study area were examined as needed to understand or define relationships inside the study area. The plume outline was derived by Steve Young (HGL) by integrating four dxf files that were provided by Kelly AFB for solvent contours of PCE, TCE, DCE, and VC based on 2001 field data. The MCL's for PCE, TCE, DCE (1,2-cis DCE), and VC are 5 ppb, 5 ppb, 70 ppb, and 2 ppb, respectively. Area of plume with total solvent concentrations above MCL's is drawn by tracing PCE and TCE 5-ppb contours. The 70-ppb DCE and 2-ppb VC contours are within those PCE and TCE contours.



Figure 3. Generalized geologic map showing the geometry of surficial deposits and the recharge and transition zones of the Edwards aquifer with respect to the study area. The recharge and transition zones are extracted from digital data (Texas Natural Resource Conservation Commission, 2001), and the distribution of alluvial sediments is excerpted from Collins (2000) and Brown and others (1974).

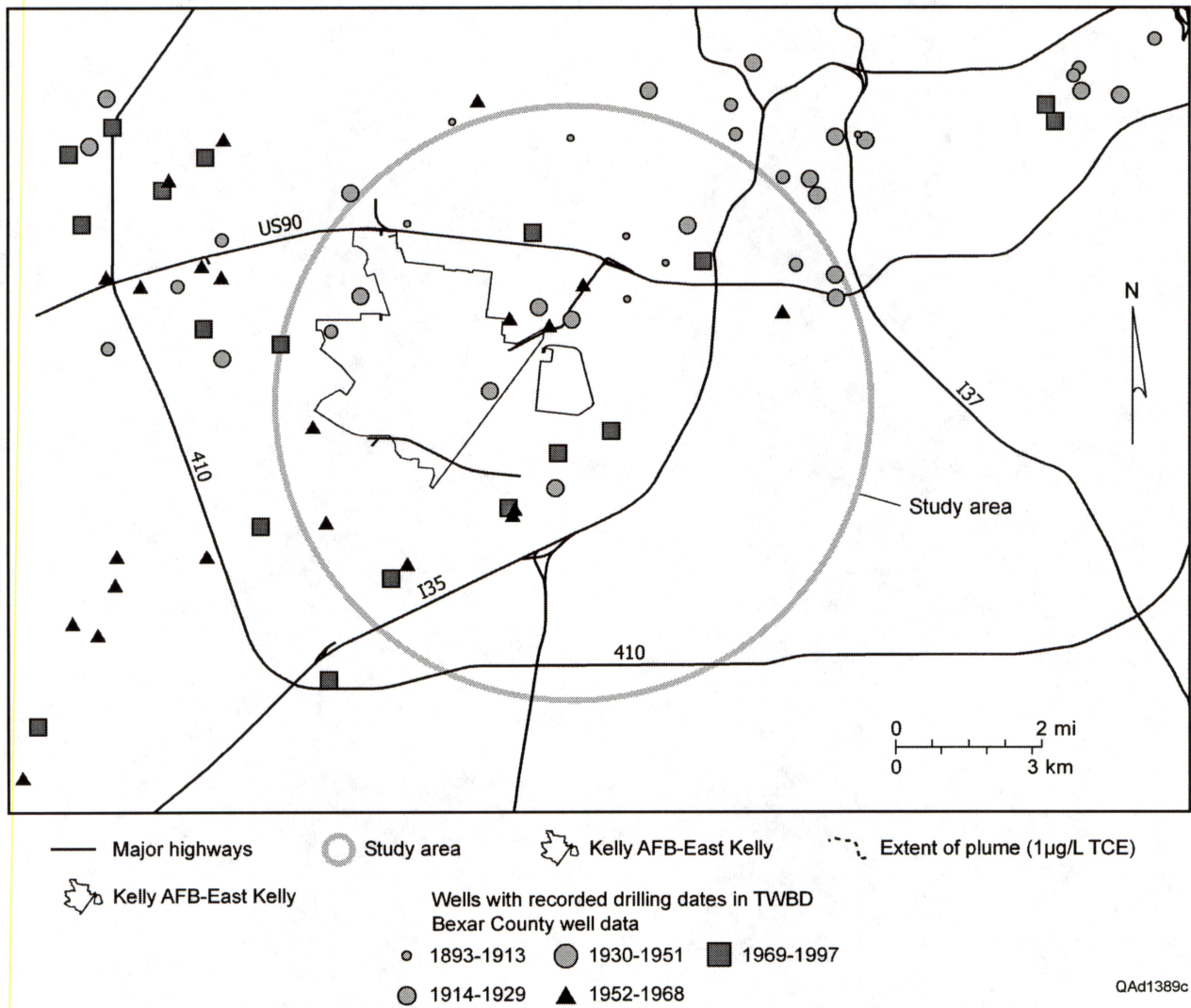


Figure 4. Distribution of known wells (Texas Water Development Board, 2002), showing drilling date, where known. Modern roads, modern Kelly outline, and study area shown for reference.

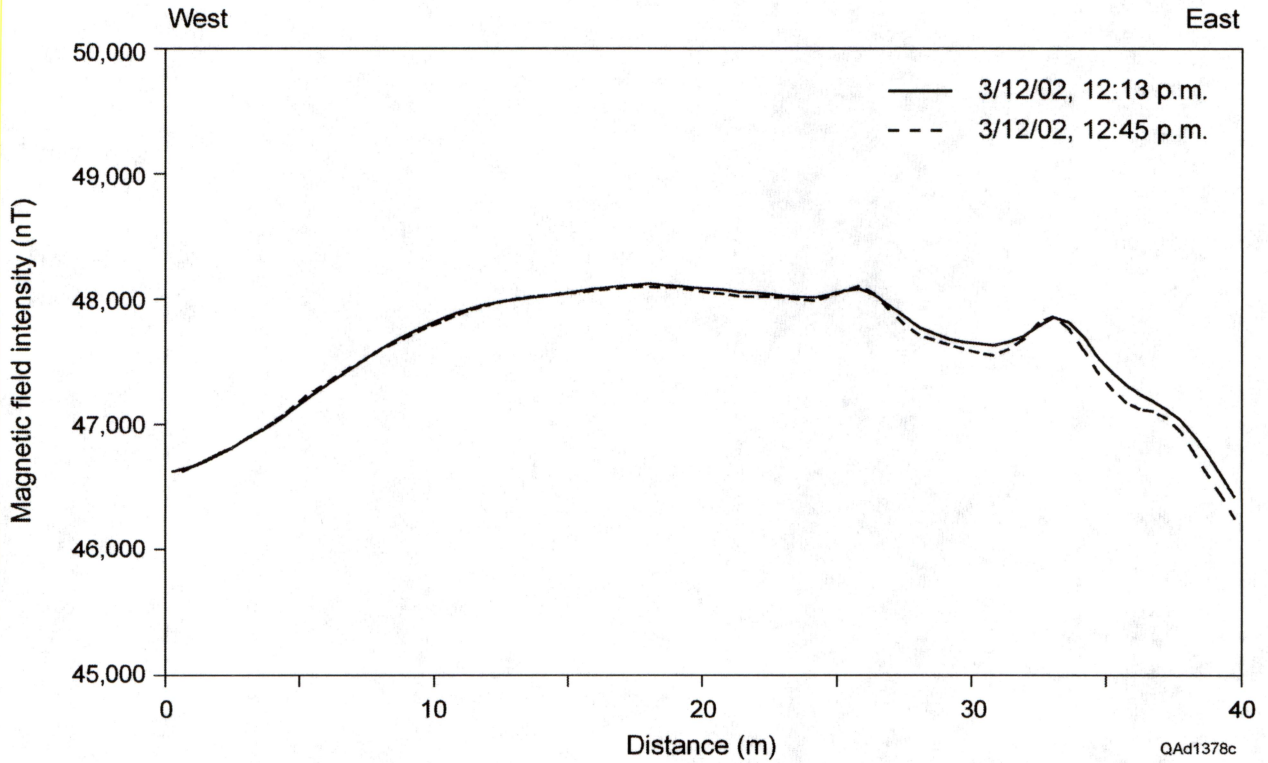


Figure 7. Comparison of magnetic field strength across the south end of the survey area before and after line data were acquired.

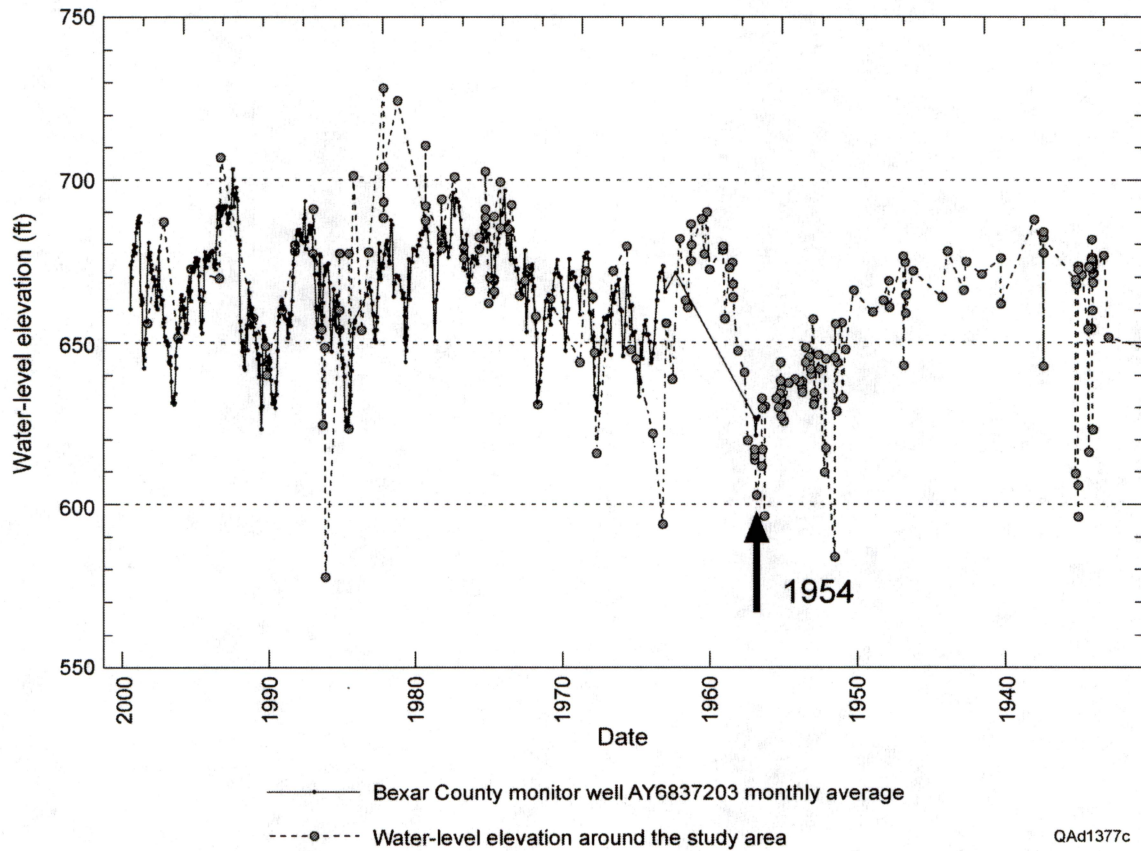


Figure 8. Water-level elevation in the study area (Texas Water Development Board, 2002) plotted versus Julian day. For comparison, the monthly water-level elevations in the Bexar County monitor well (AY6837203) are plotted on the same scale. The 1954 synoptic survey is shown at the arrow.

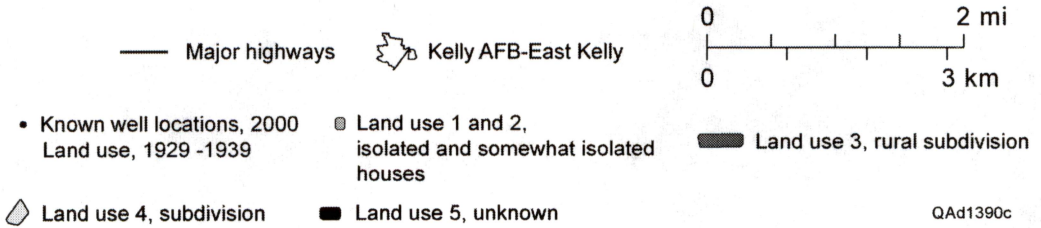
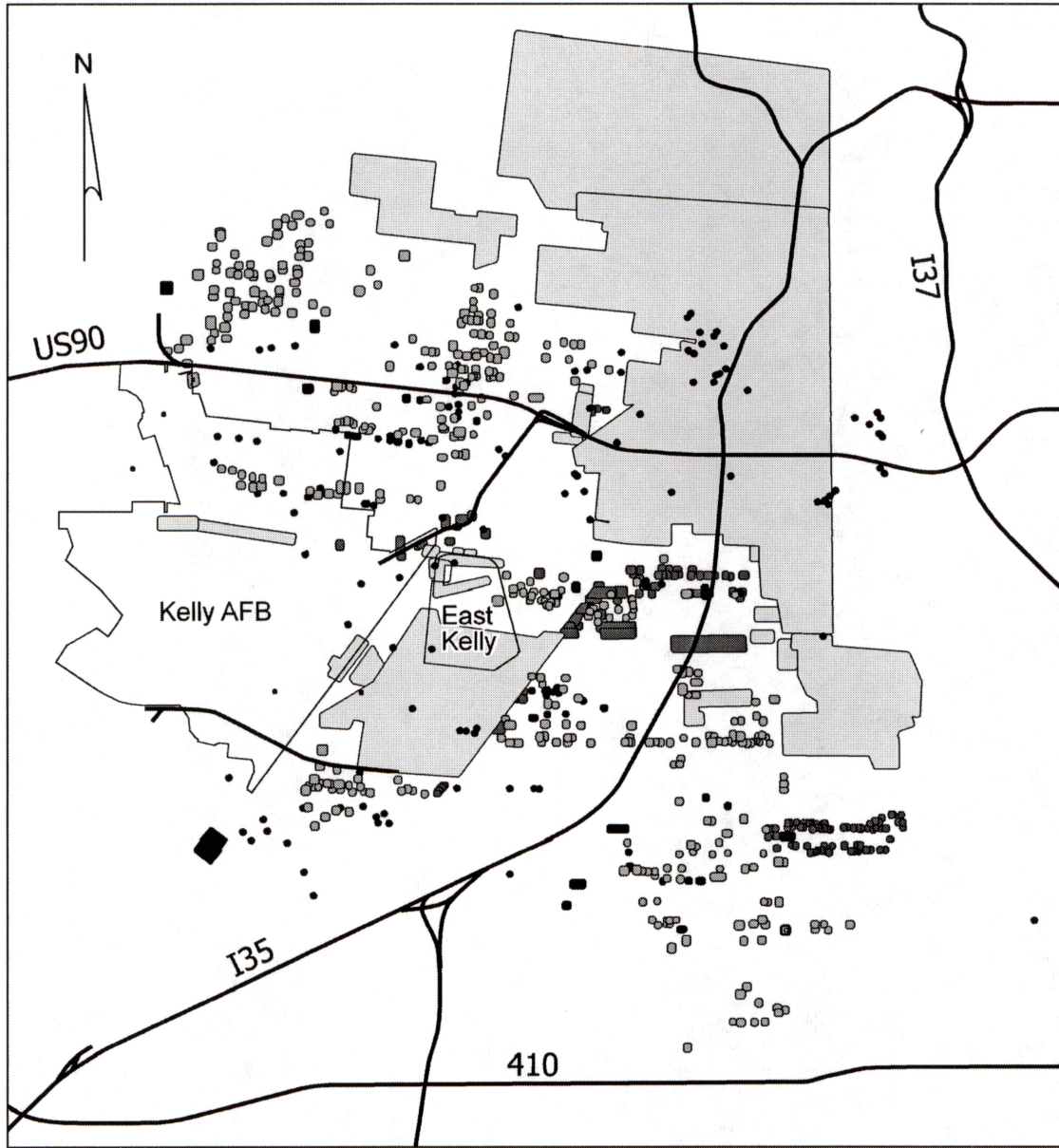


Figure 9. Historical 1929–1939 land use classification, with 35-m buffer applied, and known well locations (Science Applications International Corporation, 2000).

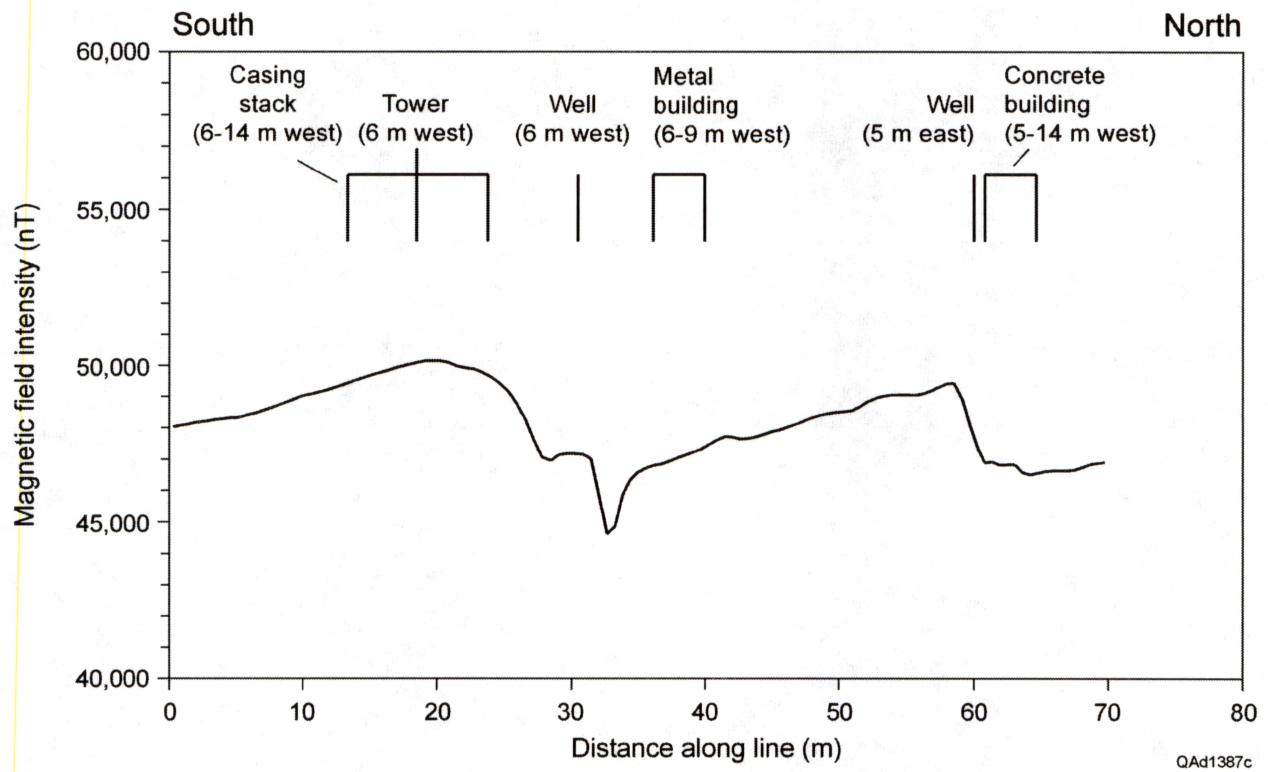


Figure 11. Magnetic-field strength along line 3. Line location shown in figure 10.

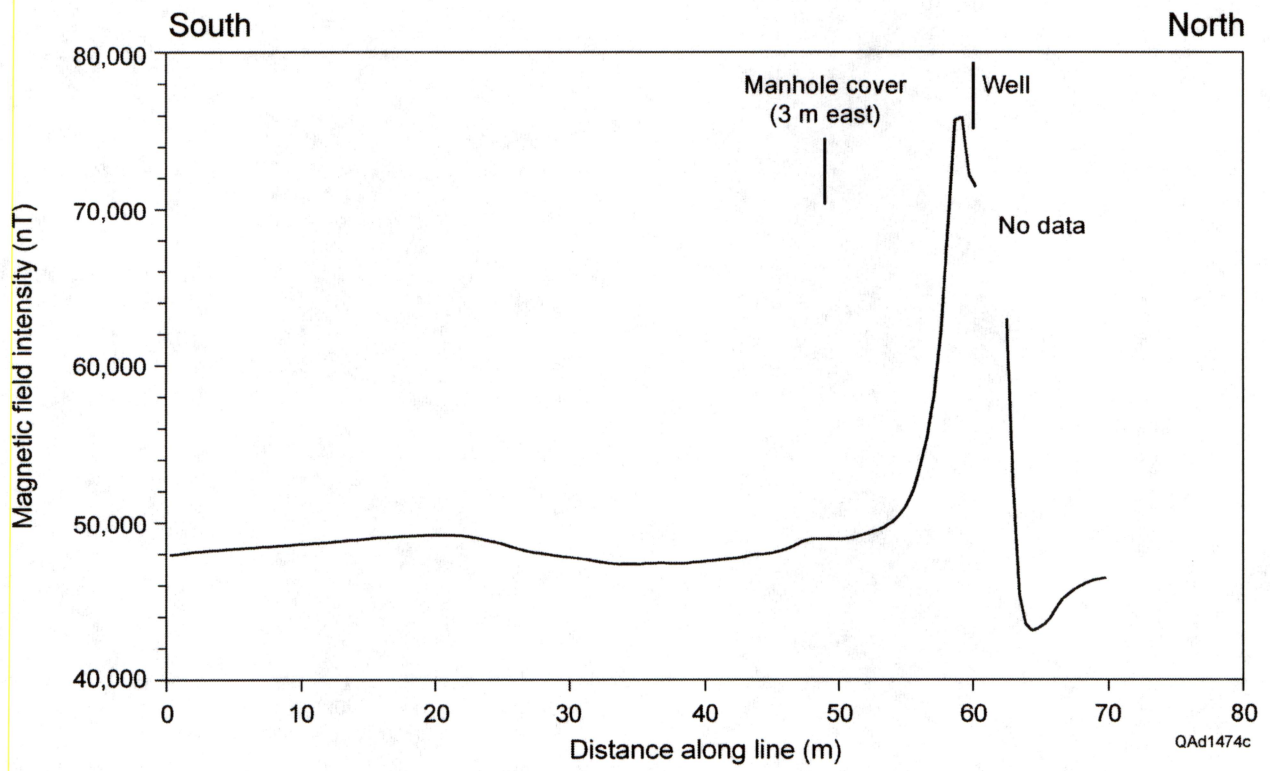


Figure 12. Magnetic-field strength along line 4. Line location shown in figure 10.

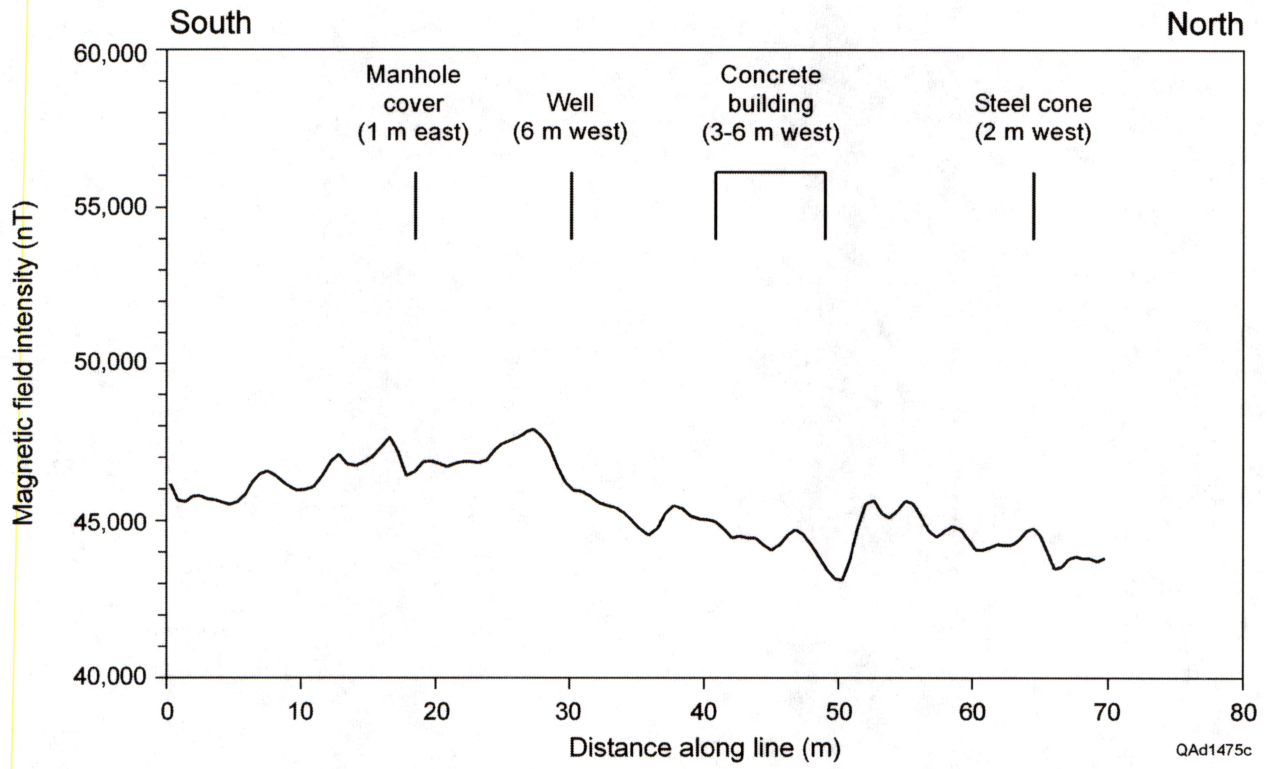
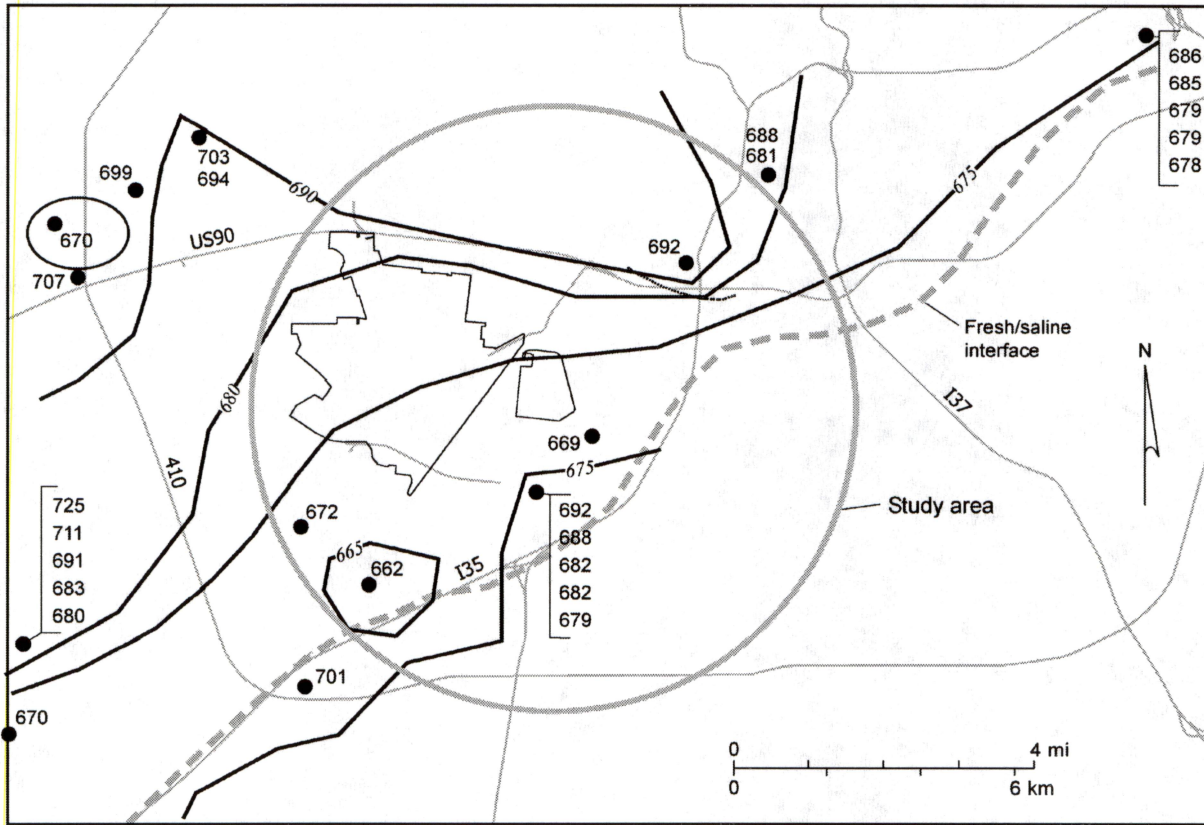


Figure 13. Magnetic-field strength along line 8. Line location shown in figure 10.



630 ● Wells measured during high aquifer stage (water-level elevation in feet)

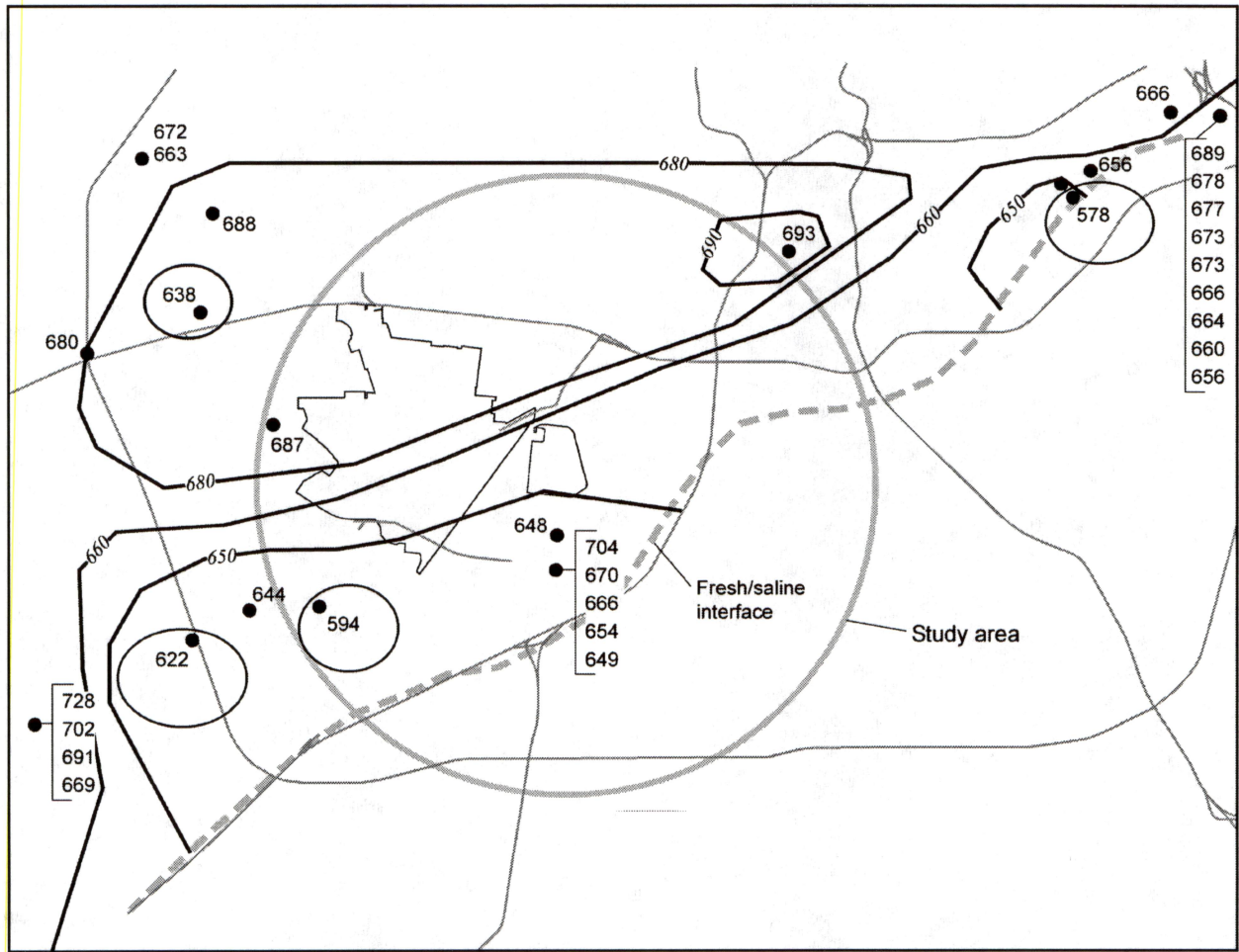
--- Fresh/saline interface

○ Study area

630 Potentiometric surface (feet)

QAd1380c

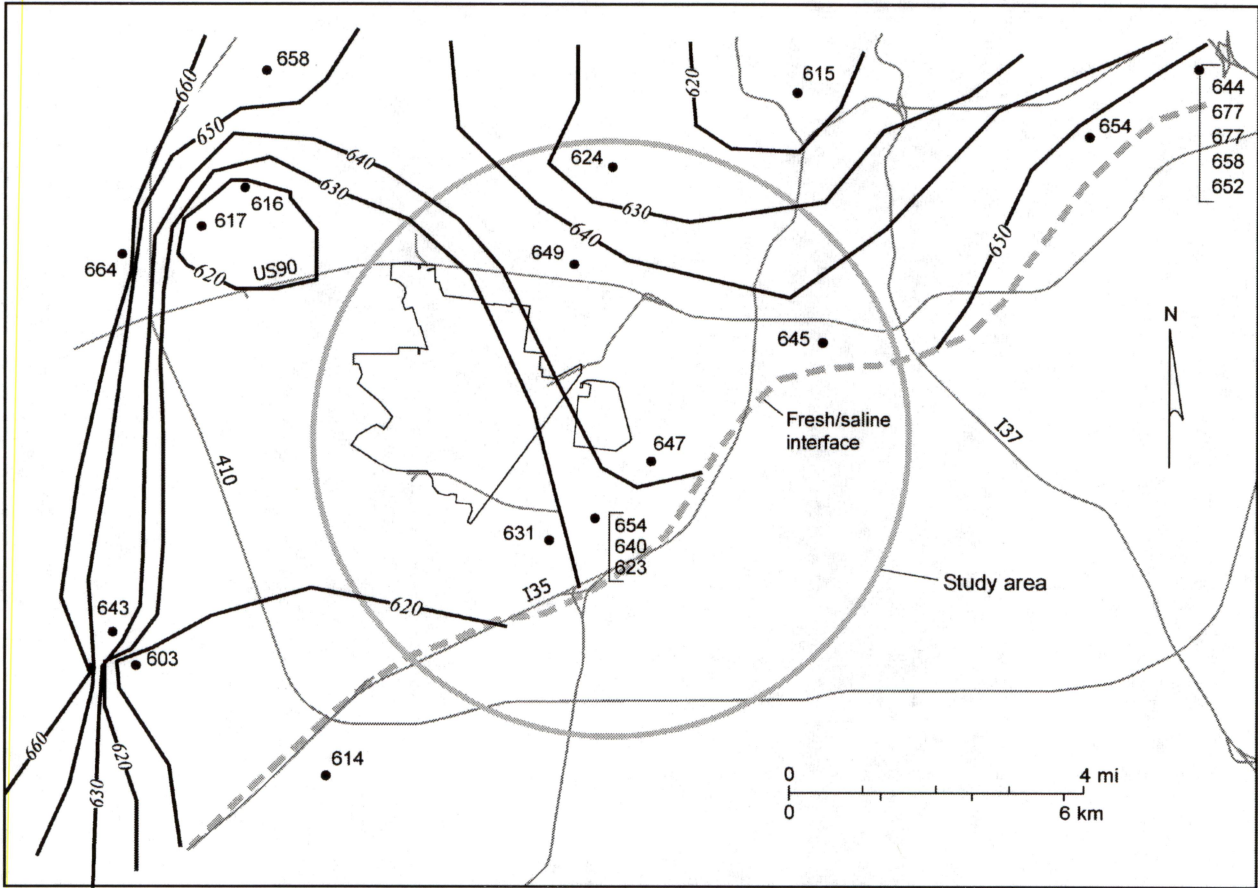
Figure 15. Potentiometric map on the Edwards high pseudosynoptic water levels. Outlier values not included in the contour are circled. Study area shown for reference. Fresh/saline interface is excerpted from Schultz (1994).



630 ● Wells measured moderate water levels (water-level elevation in feet) - - - Fresh/saline interface ○ Study area -630- Potentiometric surface (feet)

QA41381c

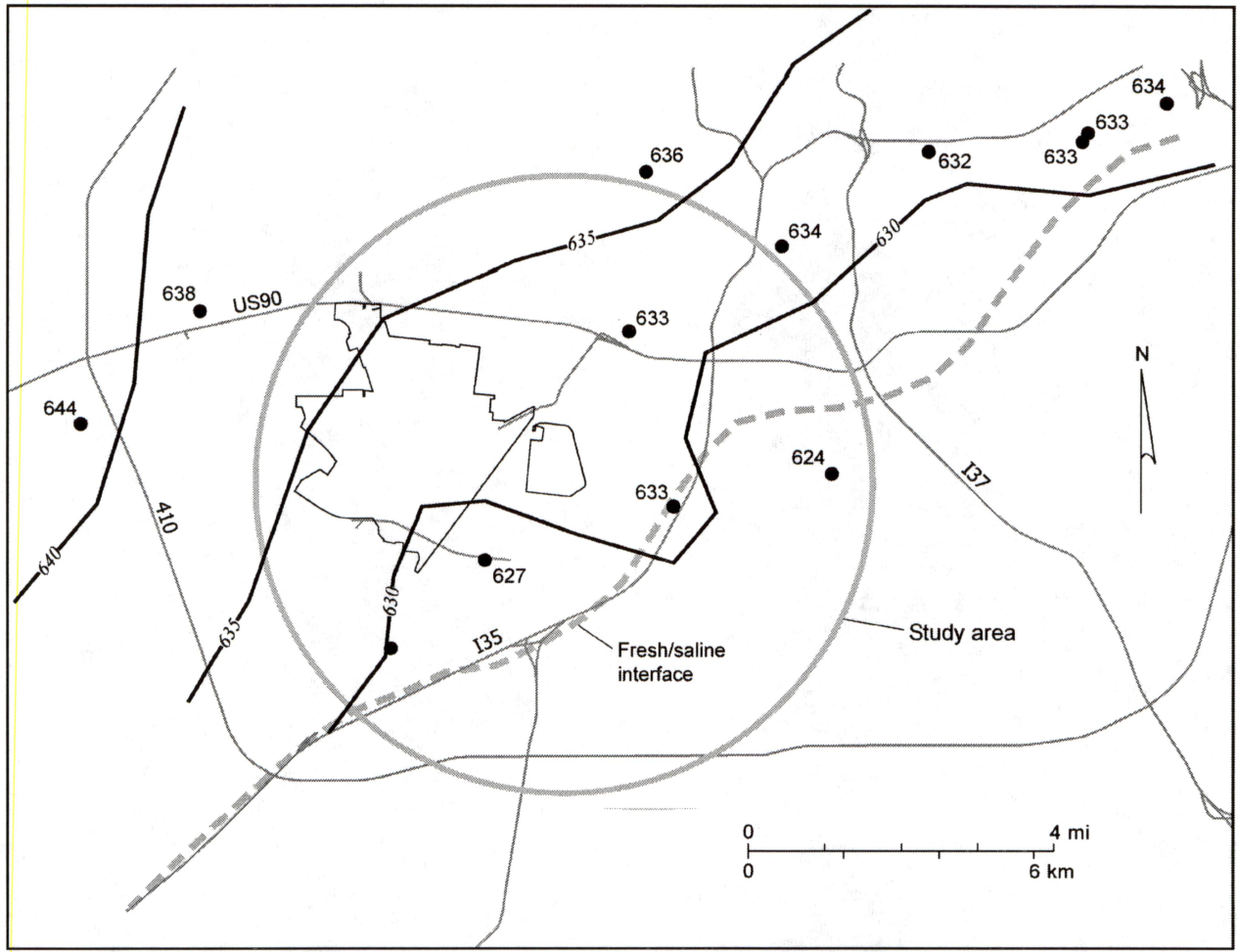
Figure 16. Potentiometric map of the Edwards moderate pseudosynoptic water levels. Outlier values not included in the contour are circled. Study area shown for reference. Fresh/saline interface is excerpted from Schultz (1994).



- Wells measured low water levels (water-level elevation in feet)
- - - Fresh/saline interface
- Study area
- 630 Potentiometric surface (feet)

QAd1382c

Figure 17. Potentiometric map of the Edwards low pseudosynoptic water levels. Outlier values not included in the contour are circled. Study area shown for reference. Fresh/saline interface is excerpted from Schultz (1994).



- Wells measured 1954 synoptic water levels (water-level elevation in feet)
- - - Fresh/saline interface
- Study area
- 630— Potentiometric surface (feet)

QAd1383c

Figure 18. Potentiometric map of the Edwards 1954 synoptic water level. Study area shown for reference. Fresh/saline interface is excerpted from Schultz (1994).

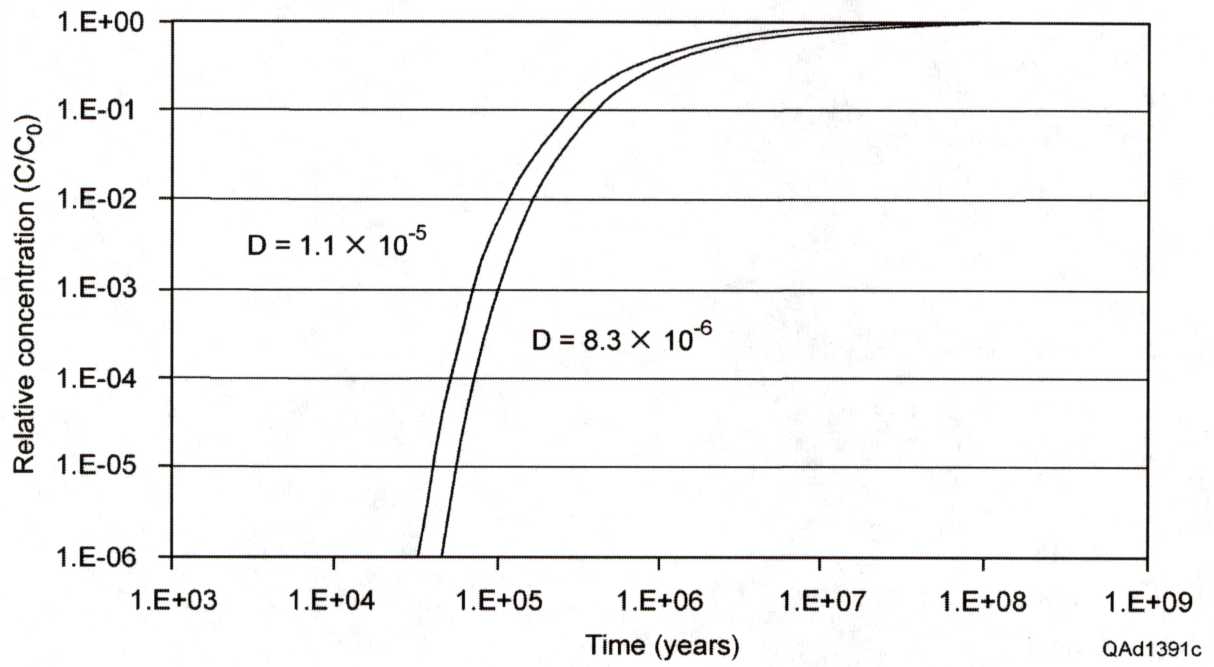


Figure 22. Relative organic compound solute concentration with time at the end of an 800-ft-length pipe with diffusion as the only transport mechanism.

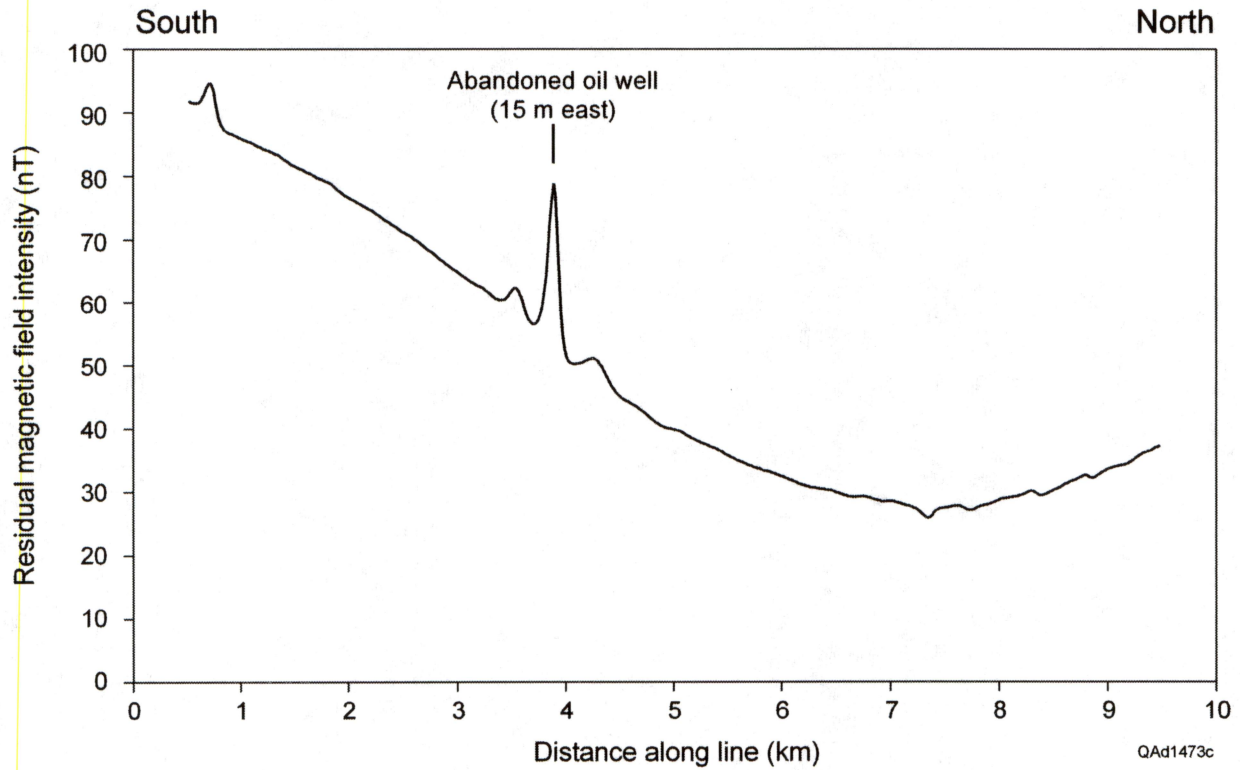


Figure 24. Normalized magnetic field strength along flight line 225 near Sterling City, Texas. Also shown is the position of an abandoned oil well projected onto the flight line.